

6 B A THERMAL MODEL AND PARAMETRIC
INVESTIGATION OF ELECTROCHEMICAL
DISCHARGE MICROWELDING

By
SARMISTHA PARIJA

ME TH
me/1993/m
1993 P 217t



M
PAR
THE

DEPARTMENT OF MECHANICAL ENGINEERING
INDIAN INSTITUTE OF TECHNOLOGY KANPUR
JANUARY 1993

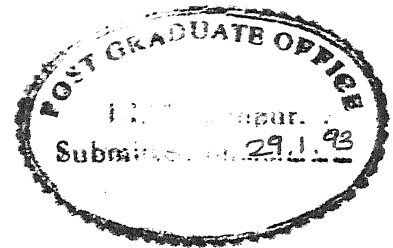
A THERMAL MODEL AND PARAMETRIC INVESTIGATION OF ELECTROCHEMICAL DISCHARGE MICROWELDING

*A Thesis Submitted
in Partial Fulfilment of the Requirements
for the Degree of*
MASTER OF TECHNOLOGY

By
SARMISTHA PARIJA


to the
**DEPARTMENT OF MECHANICAL ENGINEERING
INDIAN INSTITUTE OF TECHNOLOGY KANPUR**
JANUARY 1993

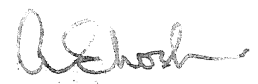
*Dedicated to
my parents*



CERTIFICATE

This is to certify that the present work entitled "A THERMAL MODEL AND PARAMETRIC INVESTIGATION OF ELECTROCHEMICAL DISCHARGE MICROWELDING" has been carried out by Sarmistha Parija under our supervision and has not been submitted elsewhere for a degree.


Mohan K. Muju
Professor


Amitabha Ghosh
Professor

Department of Mechanical Engineering
Indian Institute of Technology
Kanpur - 208016

CENTRAL LIBRARY
IIT KANPUR

~~114869~~

~~ME-1993-MAS-~~

ME-1993-M-PAR-THE

ABSTRACT

Use of electrochemical discharge phenomenon in the field of microwelding of thin wire is a very recent technique. Only one researcher [1] reported about the feasibility of the above technique. Though the ECD phenomenon is reasonably well understood, use of the phenomenon in microwelding is yet to be investigated.

The present work is planned with two main objectives,
(a) the significance of the various process control parameters and its optimum values suitable for ECD microwelding.
(b) to develop a simple realistic and quantitative model capable of predicting the time required for the welding. With above objectives an experimental setup is designed and developed.

The optimum depth of immersion of twisted wires in the electrolyte of different material composition and of different diameters were found out. A few comments are made on the significance of process parameters and on the effect of governing forces in microwelding. The theoretically predicted values from the thermal model developed give a reasonably good agreement with the experimental observations.

ACKNOWLEDGEMENT

The author expresses her deep sense of gratitude to Prof. Amitabha Ghosh and Prof. Mohan K. Muju of Mechanical Engineering Department for their valuable suggestions in the problem. Their constant guidance and encouragement really motivated me to complete my thesis work.

I am grateful to Prof. M.M. Oberoi of Mechanical Engineering Department, who shared his valuable time in helping me while deriving the thermal model. I extend my thanks to Dr. R.K. Ray of Metallurgical Department for his help during my work.

I am thankful to Mr. V. Raghuram, Research Engineer in the Department and Sushma, Research Engineer in the Center for Robotics for their help in developing the electrical circuit required for the experiments.

The author is thankful to the staff of the Manufacturing Science Laboratory M/s R.M. Jha, O.P. Bajar, P.P. Gupta, N.D. Mukhe, special thanks to Mr. H.P. Sharma for help he rendered during the experimentation.

I am grateful to all faculty members in the Manufacturing Science Laboratory for their cooperation during work both mentally and physically. I am very much thankful to my labmates

especially to Koshy, Modi, Premshankar, sameer and sandhya.

I extend my thanks to the administration of college of Engineering and technology, Bhubaneswar and Ministry of Human Resource Development, Government of India for sponsoring to pursue M.Tech study under the Quality Improvement Programme.

I am thankful to Mr. U. Mazumdar for typing the thesis.

I express my thanks to Sailaja, Anupam, Satyabrata and Y.P. for making my life at IIT Kanpur a memorable one. Finally special thanks to Dr. P.C. Das and his family.

Sarmistha Parija

CONTENTS

	TITLE	PAGE
CHAPTER I	INTRODUCTION	1
1.1	ECD Microwelding	1
1.2	Electrochemical and Electrodischarge Process	2
1.3	Electrochemical Discharge (ECD) Phenomenon	4
1.4	Mechanism of ECD Phenomenon	7
1.5	Discharge Always at Bottom Edge of Cathode (Why?)	11
1.6.1	Survey of Previous Work	15
1.6.2	Review of ECDW	19
1.7	Objective and Scope of the Present Work	26
CHAPTER II	EXPERIMENTAL INVESTIGATION OF ECD WELDING	
2.1	Introduction	28
2.2	Description of the Experimental Setup	29
2.3	Electrolyte Type Selection	32
2.4	Thermocouple Wire Materials and sizes	33

2.5	Effect of Electrolyte Concentration	35
2.6	General Characteristics of ECD Welding	37
2.7	Effect of Wire Diameter	42
2.8	Effect of Material Composition on Microwelding	45
2.9	Effect of Variation in Voltage on Microwelding	45
2.10	Microwelding of Platinum (10%Rh)-Pt, Copper - Copper, Constantan - Copper wires	49
2.11	Mechanism of Microwelding	52
2.12	Mechanism of Void Formation.	52
2.13	Satisfactory Welding Zone as a Function of Voltage with D.C. Smooth Power Supply	55
2.14	Comparison of calibration chart	57
CHAPTER III THERMAL ASPECTS: THEORETICAL ANALYSIS EXPERIMENTAL VERIFICATION		
3.1	Indroduction	60
3.2	Theoretical Model	61
3.2.1	Assumptions	61
3.2.2	Problem Formulation	63
3.2.3	Numerical Evaluation of the Solution	66
3.3	Experimental Verification of the	70

Model	
3.3.1 Experimental Setup	70
3.3.2 Modified Experimental Method	71
3.3.3 Evaluation of the Time for Bead Centre to Attain Melting Temperature	74
3.3.4 Effect of Diameter on Melting Time	77
3.3.5 Effect of Applied Voltage and Concentrations	77
3.4 Summarization of the Results	82
CHAPTER IV CONCLUDING REMARK AND SCOPE FOR FUTURE WORK	
4.1 Discussion on the results obtained from ECD microwelding experiments.	83
4.2 Dissscussion on thermal model,theoretical and experimental aspects.	85
4.3 Limitations of the present work and for further research.	87
REFERENCES	89
APPENDIX-1	92
APPENDIX-2	96

LIST OF FIGURES

- 1.1 A simple thermoelectric pyrometer
- 1.2 Dimensions of a thermocouple bead
- 1.3 Voltage and current density ranges of the machining systems using electrolyte solutions[1]
- 1.4 Schematic diagram of ECD set up
- 1.5 Bubble density on -ve electrode at different applied voltage[2]
- 1.6(a) Discharge location with bubble distribution at critical condition[2]
- 1.6(b) Idealised switching off situation[2]
- 1.7(a) Accumulation of opposite charges at the interface[2]
- 1.7(b) Equivalent electric ckt of the ECDsetup[2]
- 1.8 Distribution of I near a sharp edge[2]
- 1.9 Bubble blockage at the bottom edge of the electrode
- 1.10 Effect of the electrolyte flow on V [1]
- 1.11 Distribution of voltage drop in an ECD bath
- 1.12 Resistance in ECD configuration[1]
- 1.13 Voltage vs electrolyte concentration in ECD

- microwelding[1]
- 1.14 Schematics of microwelding setup[1]
- 1.15 V-I characteristics for different type
of power supply[2]
- 1.16 V-I characteristics for different tool
depth[2]
- 1.17 V-I characteristics for different tool
diameters[2]
- 1.18 Critical voltage and current at different
concentration
- 2.1 Experimental setup for ECD microwelding
- 2.2 Variation of voltage parameters with
electrolyte concentration
- 2.3 Variation of current parameters with
electrolyte concentration
- 2.4 Waveshape of voltage and current with
inductor in the circuit
- 2.5 Waveshape of voltage and current with
capacitor in the circuit
- 2.6 Waveshape of voltage and current with
capacitor and inductor in the circuit
- 2.7 Variation of imersed depth with wire
diameter for different material composition

- 2.8 Variation of immersed depth with diff
wire diameter of different matl. composition.
- 2.9 Loss of material from bead with diferent
diameter at different voltages
- 2.10 Variation in depth of immersion vs diameter

of wire.
- 2.11 Stages in mirowelding
- 2.12 Mechanism of void formation
- 2.13 Nature of voltage-electrolyte concentration
in microwelding
- 2.14 Comparison between standard temperature
millivolt calibration graph and that
obtained by ECD weld bead
- 3.1 Circular heat source around the bottom
edge of the electrolyte
- 3.2 Representation of wire in cylindrical
coordinate system
- 3.3 Procedure for the measurment of time reqd
by cathode wire to reach the melting temp
- 3.4(a) Variation of temp w.r.t time obtained
experimentally
- 3.4(b) Comparison of observed and calculated time for

- cathode wire to reach melting temp
- 3.5 Experimental & theoretical pattern showing nature of variation of temperature with time in ECD microwelding
- 3.6 Time to reach melting temp as a wire as a function of wire diameter
- 3.7 Time to reach melting temp vs electrolyte concentration
- 3.8 Variation of $t(m)$ with applied voltage at different concentration
- 3.9 Comparison of $t(m)$ vs applied voltage at different electrolyte concentration
- A-1 Evaluation of $l(i)$

NOMENCLATURE

A_e	-	equivalent active area of electrode [cm^2]
C_1, C_2, C_3	-	capacitance
D	-	diameter of the welded bead [mm]
d	-	diameter of wire electrode [mm]
I	-	current [A]
J	-	current density [A cm^{-2}]
k	-	thermal conductivity of wire cathode, $\text{J/s} \cdot \text{m} \cdot ^\circ\text{C}$
K_2	-	co-efficient for determining R_{2c} [$\Omega \text{ cm}^2 \text{ mole}^{-0.5}$]
K_3	-	co-efficient for determining R_{3c} [$\Omega \text{ cm}^2 \text{ mole}^{-1.0}$]
L	-	inductance
l	-	length of tool electrode dipped in electrolyte [cm]
l_1	-	imaginary extension of tool electrode [cm]
l_e	-	$(l + l_1)$, equivalent length of tool electrode [cm]
M	-	mole fraction
m_1	-	no. of moles of solvent
m_2	-	no. of moles of solute
Q	-	rate of heat input [cal/s]
R_{1c}, R_{2c}, R_{3c}	-	resistance [Ω]
$T(t)$	-	actual temperature of bead [$^\circ\text{K}$]
t	-	time [s]
V	-	applied voltage [V]

- v - total volume of gas [cm^3]
- α - thermal diffusivity [cm^2/s]
- α_0 - co-eff. of Faradic H_2 generation [$\text{cm}^3\text{A}^{-1}\text{sec}^{-1}$]
- δ - co-eff. of vapour generation [$\text{cm}^3\text{watt}^{-1}\text{sec}^{-1}$]
- λ_1, λ_2 - indices over mole fraction
- λ_0 - constant

Subscript

- c - critical value

CHAPTER I

INTRODUCTION

1.1 ECD MICROWELDING

Quite often very small sized welding; normally called microwelding, are essential. The usual technology employed in case of normal welding can't yield desirable results in case of microwelding. One major use of these types of weldings is in making thermocouples. Since the size of the welding is very small the process of microwelding must be more gentle with less amount of energy release taking place. Furthermore it is also necessary to have better control of energy release rate and other parameters in case of microwelding. Allesu [1] was the first to show that electrochemical discharge phenomenon can be effectively employed for microwelding of thin wires. Though he didn't investigate in details the mechanism of the process his experiments showed that not only was the quality of such microwelded joints very good the arrangement required for the process is extremely simple without requiring any expensive equipment.

As mentioned earlier one of the major usage of this microwelding technique is the production of thermocouples. The thermocouple is the main component of the thermoelectric pyrometer (Fig. 1.1) whose operation principle is based upon seebeck effect.

The thermocouple is the joining of two dissimilar metallic wires which develops an emf when there is a temperature difference between their junction points. The thermocouple wires should be in electrical contact (as shown in Fig. 1.2) only at the bead which forms the hot junction. If the wires are also in contact at other points along the length, then the e.m.f. indicated will be in error due to induction effect, as explained further in section-3.3.1. Thermocouples are manufactured to have a smooth well-rounded welded bead. The conventional flame-method is very cumbersome to prepare a nice bead.

1.2 ELECTROCHEMICAL AND ELECTRO DISCHARGE PROCESSES

The usefulness of electrolysis phenomenon to produce polished surface was first noticed by Jacquet and subsequently W. Gusselt of USSR in 1935 and Burgess of USA in 1941 developed the process into present day ECM.

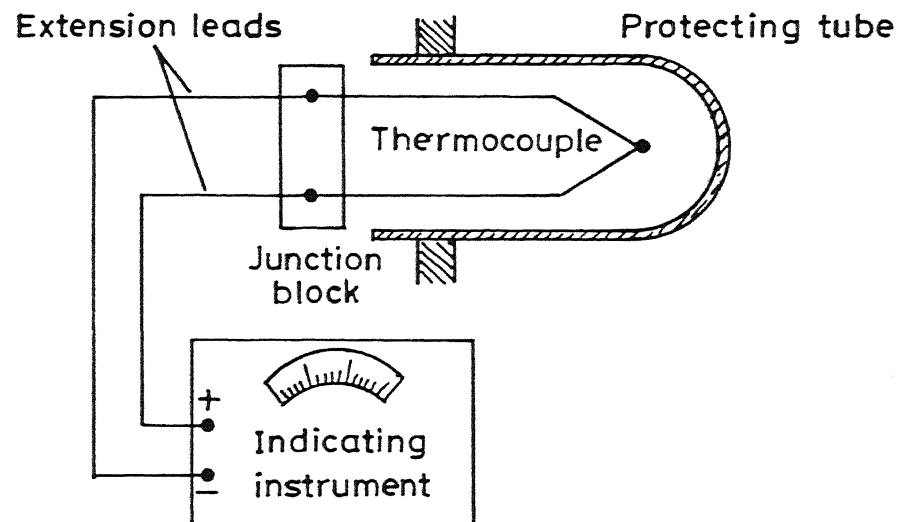
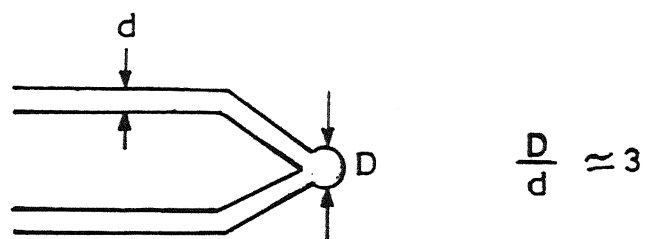


Fig.1.1 A simple thermoelectric pyrometer .



d – diameter of individual wire
 D – diameter of the thermocouple bead

Fig.1.2 Dimensions of a thermocouple bead .

The credit of inventing the technique of EDM, should go to the ENGLISH scientist pristley and Lazarenko and Lazarenko of USSR. Pristley detected the erosive nature of electric spark in the dielectric, Lazarenko and Lazarenko established it as a machining process in 1943.

In the early 70's a hybrid process was conceived in which the phenomenon of electro-chemical discharge was employed for the removal of material. This hybrid process for electrically conducting work material is known as electrochemical arc machining (ECAM) and that for electrically non-conducting material as electrochemical discharge machining (ECDM). Figure 1.3 illustrates the ranges of voltage and current density of various system of machining using electrolyte. Usual voltage ranges of ECM is 8 to 20 volts and that for ECAM is 20 to 40 volts. Very high current density is attained by ECAM process upto value of 8000A/cm^2 and consequently a high MRR is achieved. The MRR in ECAM can be upto five times that in ECM and about forty times that in case of EDM. The voltage for ECDM is in the range of 30 to 100 volts depending upon the tool size, electrolyte etc.

1.3 ELECTROCHEMICAL DISCHARGE (ECD) PHENOMENON

An electrochemical cell consists of two electrodes dipped

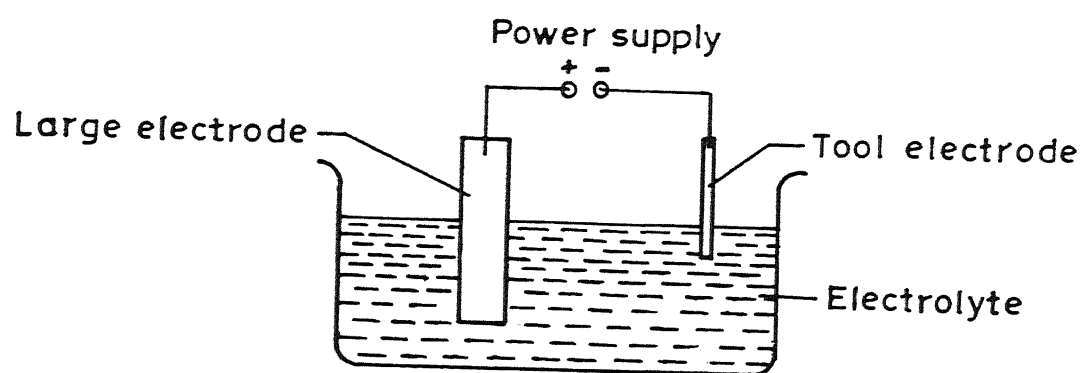


Fig.1.4 Schematic diagram of ECD set up

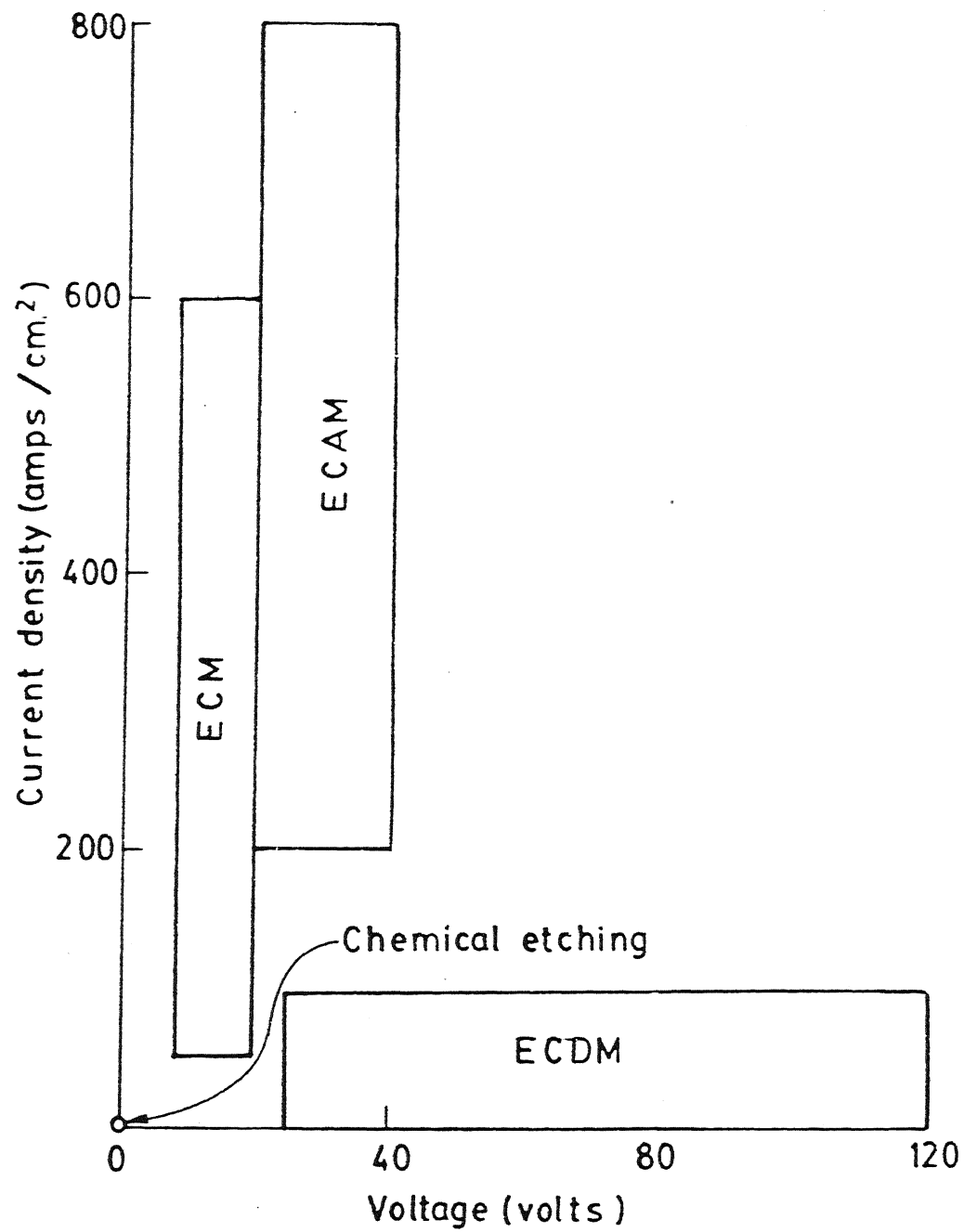


Fig.1-3 Voltage and current-density ranges of the machining systems using electrolyte solutions [1]

in an electrolyte as shown in Figure 1.4. Application of electric potential between the electrodes causes an electric current to flow through the cell resulting in electrochemical reactions, such as anodic dissolution, cathodic deposition, electrolysis of the electrolyte, gas bubble generation, etc., depending on the electrode-electrolyte combination. If the electrodes are of grossly different sizes, then, beyond a certain value of the applied potential, electric sparks appear at the bottom edge of the smaller electrode and the cell current drops. This phenomenon is known as electrochemical discharge (ECD).

1.4 MECHANISM OF ECD PHENOMENON

The vapour blanketing of the cathode electrode (smaller diameter) has been identified as the primary reason for discharge initiation. Hydrogen gas is liberated in the form of bubbles at the cathode, due to electrochemical reaction. The bubbles gradually grow in size and after attaining a critical size, they detach from the electrode surface. Nucleation site density of H_2 bubble increases with applied voltage to the cell. When the nucleation site density of H_2 becomes sufficiently high, substantial constriction of the current path takes place at the interface. Figure 1.5 shows the nucleation site density on the electrode surface at different values of the

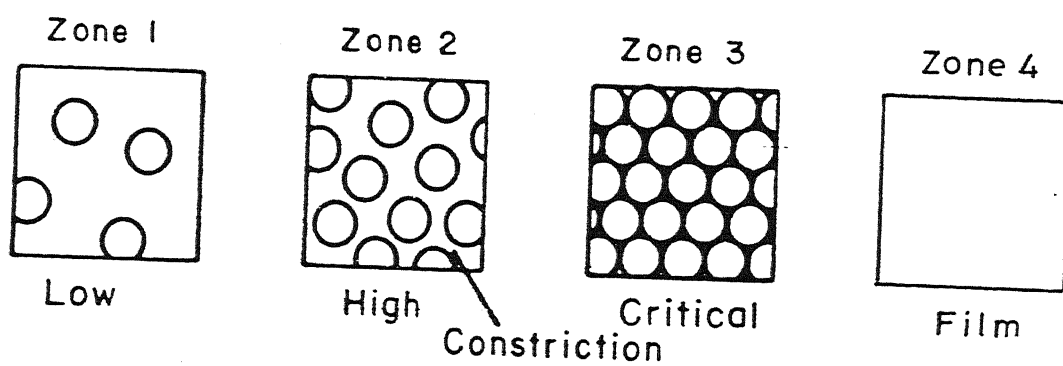
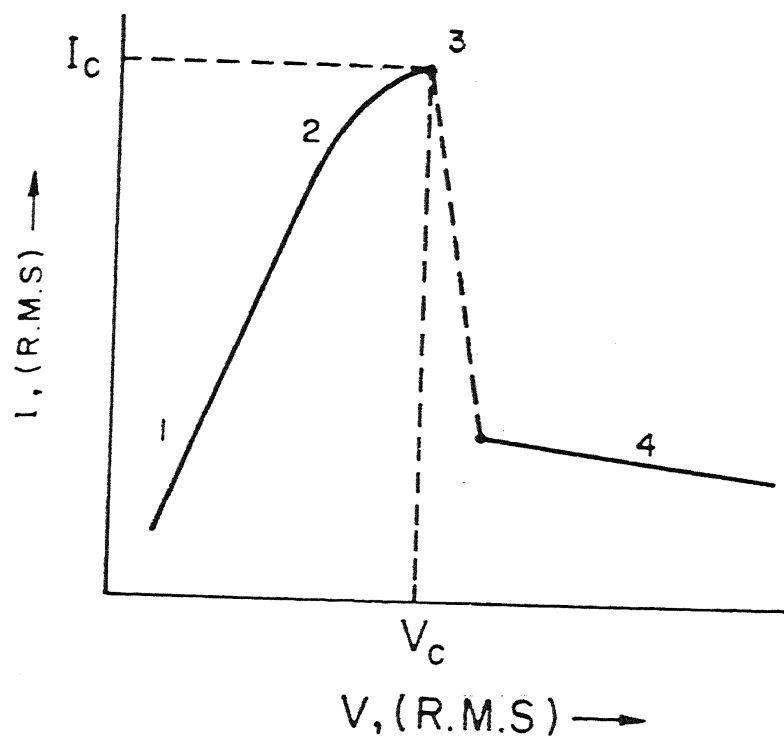


Fig.1.5 Bubble density on -ve electrode at different applied voltage.[19].

applied voltage and cell current and the location of the constrictions. This causes an increased resistance at that region and the ohmic heating of the electrolyte becomes significant. This causes the onset of vapour bubble nucleation on the electrode surface in addition to the H_2 bubbles. Beyond this state the number of combined nucleation sites increases very rapidly with the applied voltage; as observed by Janson and Hoogland [5] Allesu [1,9] investigated a number of important aspects of the ECD phenomenon. In a more recent work conducted by Basak [2] the mechanism of spark generation during ECD had been thoroughly investigated. He is the first to identify these sparks to be generated by switching phenomenon rather than break down of the gas in the vapour blanket as was thought earlier [1,19]. A major significance of this result is that the inductance in the circuit becomes an important parameter. Thus adjustment of the inductance of the circuit makes the process amenable to better control, as mentioned in his work. He noticed that at the critical value of the nucleation site density, maximum possible coverage of the electrode surface takes place with the full grown hemispherical bubbles. At this stage the points of contact between the electrolyte and the tool electrode, known as bubble, blows off instantly due to intense heating Fig. 1.6(a). Consequently, the current through the circuit drops to zero within a very short time span, which has

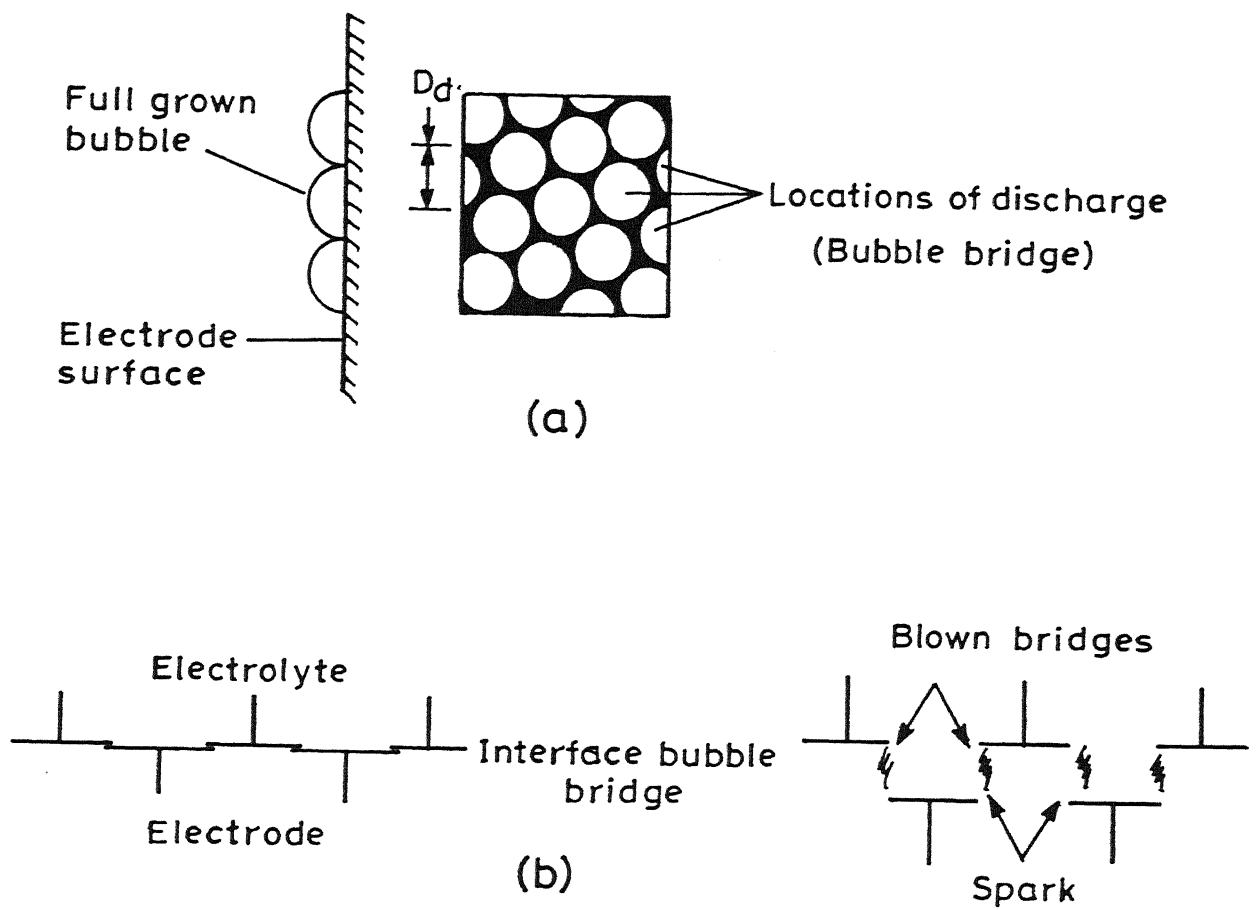


Fig.1.6(a) Discharge locations with bubble distribution at critical condition
 (b) Idealised switching off situation [2]

been identified as analogous to the switching off in an electrical circuit Fig. 1.6(b). Discharge takes place along the locations of the bubble bridge. The bubbles dislodge from the electrode surface due to bridge blowing and the contact between the electrode and the electrolyte is re-established. This cycle repeats continuously.

1.5 DISCHARGE ALWAYS AT BOTTOM EDGE OF CATHODE (WHY ?)

In this work the author has taken the mechanism of ECD proposed by Basak [2] for investigating the process of microwelding using ECD. In figure 1.4 of an ECD set up the contact area between the electrode and the electrolyte constricts due to the bubble nucleation on the electrode surface. The constriction produces the effect of an extra electrical resistance. The interionic repulsive force restricts the ion movement in the electrolyte and produces electrical resistances. The electrodes attract the oppositely charged ions due to the electrostatic force. At any instant of the process some unneutralised ion remain stagnant near the electrodes.

These oppositely charged elements separated by a small distance at the electrode-electrolyte interface is equivalent to the situation in a charged capacitor Fig.1.7 (a) The

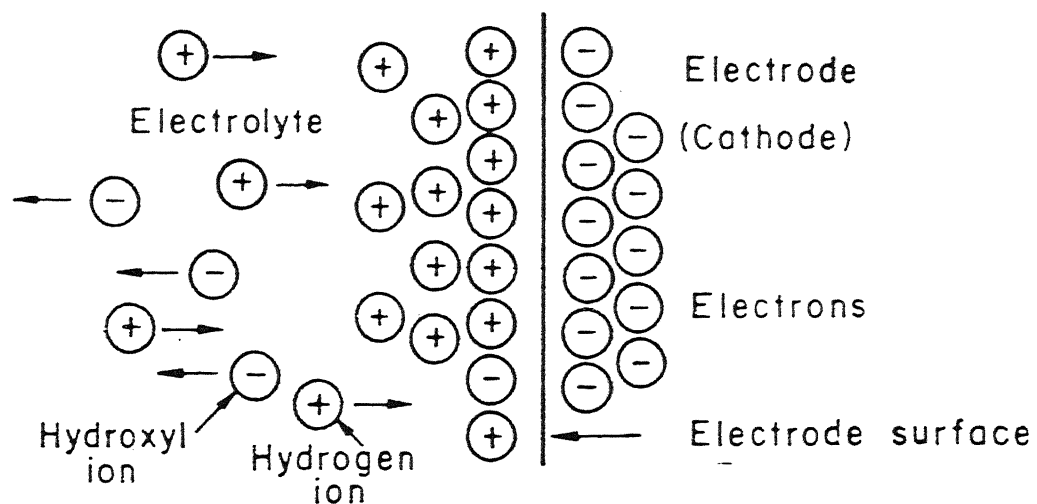


Fig.1.7(a) Accumulation of opposite charges at the interface.[2]

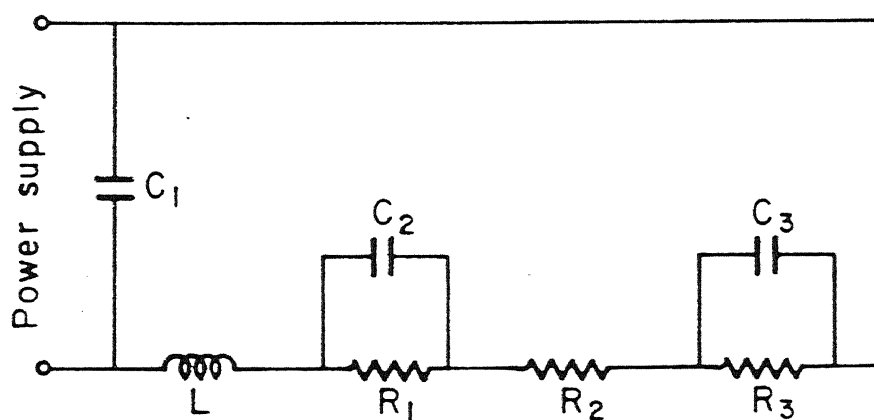


Fig.1.7(b) Equivalent electrical circuit of the E.C.D set up.[2]

constriction of the current due to the bubble formation causes nonuniformity in the current path and results in an inductive effect apart from the resistive one. Thus the circuit of an ECD set up can be represented as shown in Fig. 1.7 (b). C_1 and L are the capacitance and inductance which are inherent permanent features of the circuit. C_2 and C_3 are the capacitance values of the interfaces which arises due to the accumulation of the opposite charges at those regions. R_1 and R_3 are the resistances at the interfaces due to the constriction effect of the bubbles and R_2 is the resistance of the bulk electrolyte.

The effect of current concentration takes place if there is any sharp edge present in the current path. This disturbs the current distribution of the systems and a potential field is developed at the region. Due to this characteristics the current concentration appears at the tool edge (Fig. 1.8). As a result the discharge is mostly confined to this region. The bubbles move upward to the electrolyte surface due to the buoyant force exerted by the electrolyte. But the bubbles at the bottom surface of the electrode cannot move freely as its upward movement is restricted by the electrode surface itself (Fig. 1.9). So it can be assumed that the bottom face of the electrode is permanently insulated from the electrolyte by these stagnant bubbles. So the discharge always takes place at the bottom edge of cathode around its circumference.

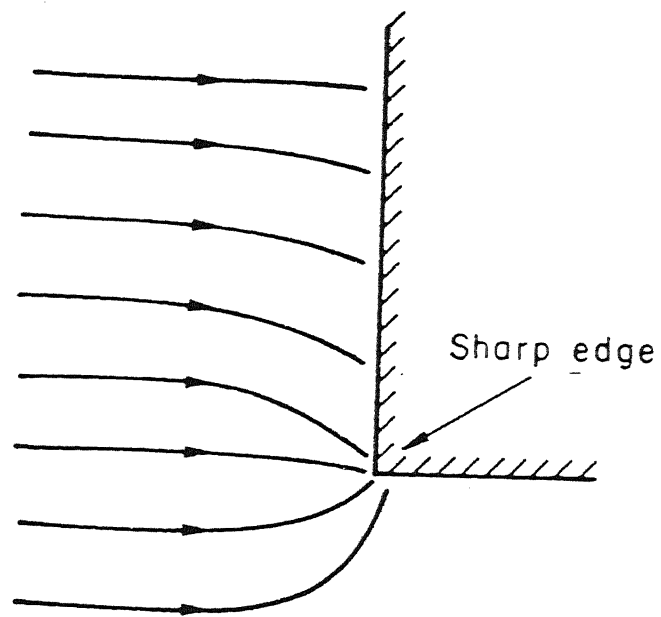


Fig.1.8 Distribution of current near a sharp edge[2]

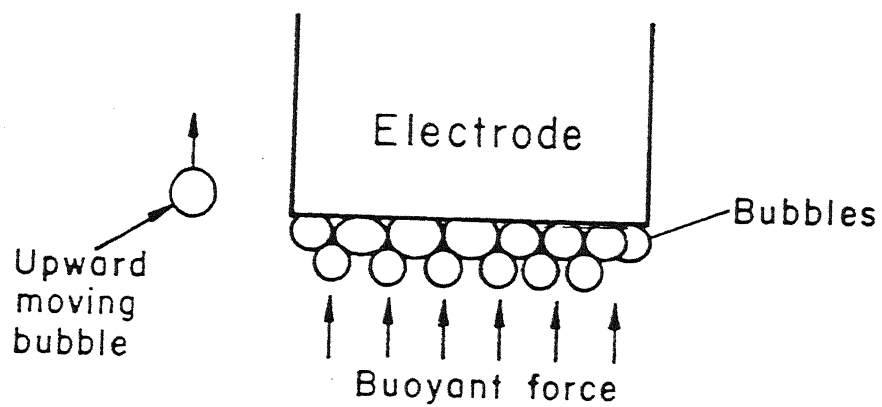


Fig.1.9 Bubble blockage at the bottom edge of the electrode.[2]

1.6.1 SURVEY OF PREVIOUS WORK

Though electrochemical arc phenomenon has been widely investigated for machining; a very limited literature is available on electrochemical discharge phenomenon. The phenomenon of small electric discharges at the anode tip was first reported by Taylor during electrolysis of molten NaCl at high current density and later Kellogg [7] showed that similar phenomenon can occur at the cathode. Cook [6] conducted experiments with ECD for machining of glass and other electrically non conducting materials and identified the applied voltage, tool polarity, electrolyte temperature and concentration as process parameters. Umesh Kumar [3,4] carried out experiments with cathode as smaller diameter electrode. He noticed that the discharge vanishes with a flowing electrolyte.

Allesu[1] conducted extensive experiments on ECD phenomenon. He examined the effect of the electrolyte flow on the discharge voltage and found that the discharge voltages increases with the electrolyte flow velocity [Fig. 1.10]. Another important observation made by him is the distribution of voltage drop in an ECD bath [Fig. 1.11] and the sources of the resistances (Fig. 1.12). McGeough and his research team conducted many experiments in the field of ECAM [11-17] and reported high material removal rate. Tsuchiya [18] drilled

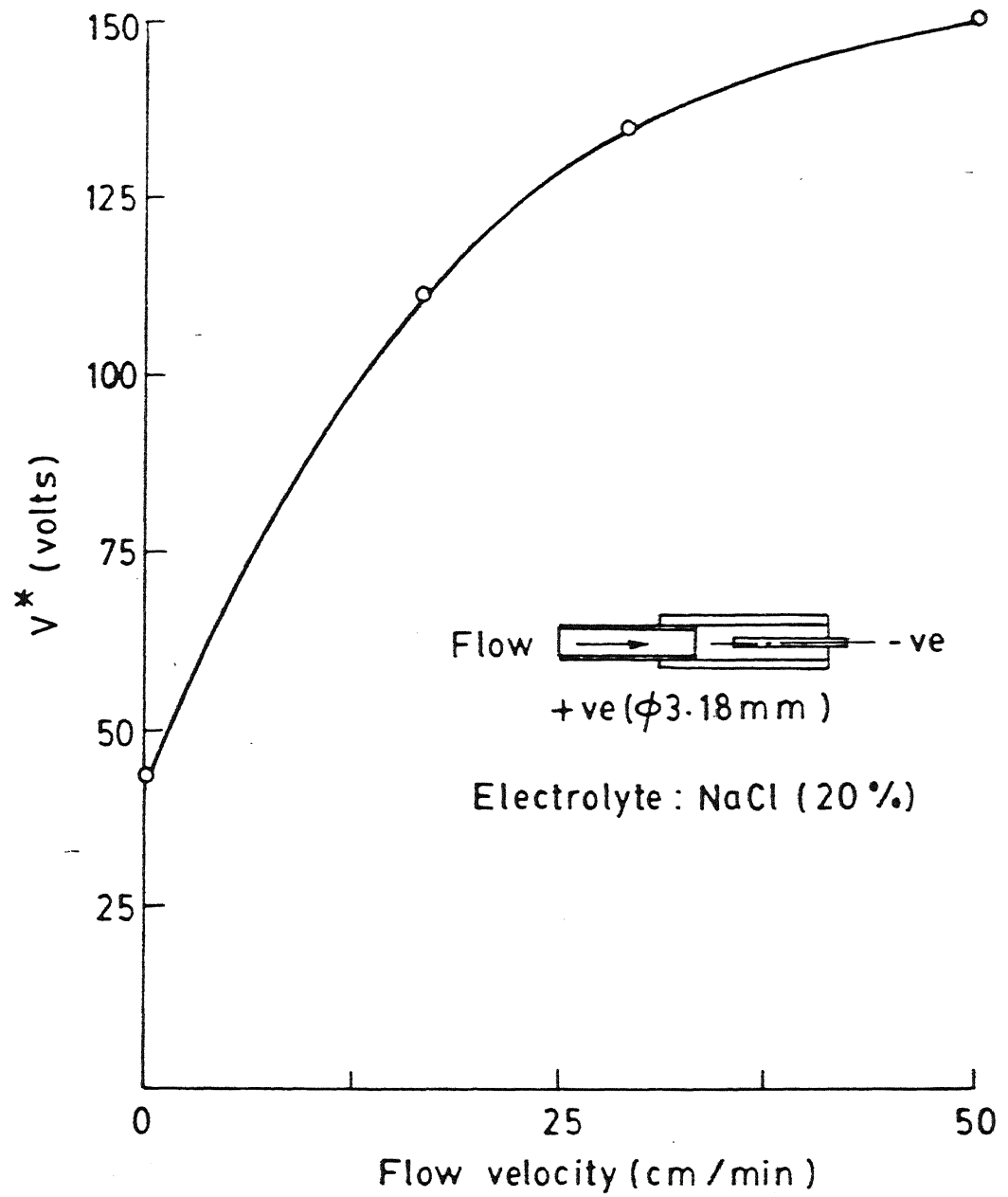


Fig.1.10 Effect of the electrolyte flow on V^* [1]

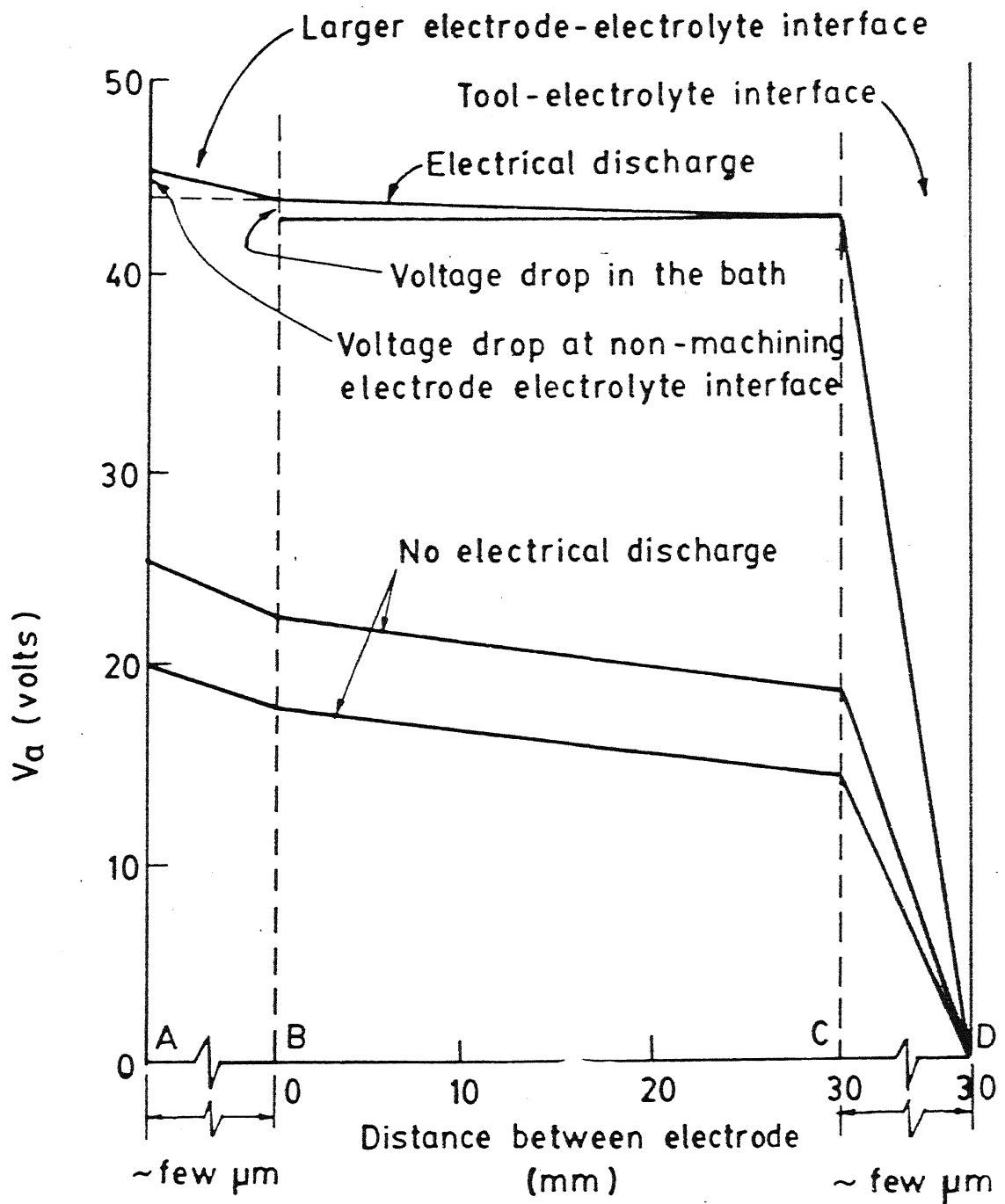
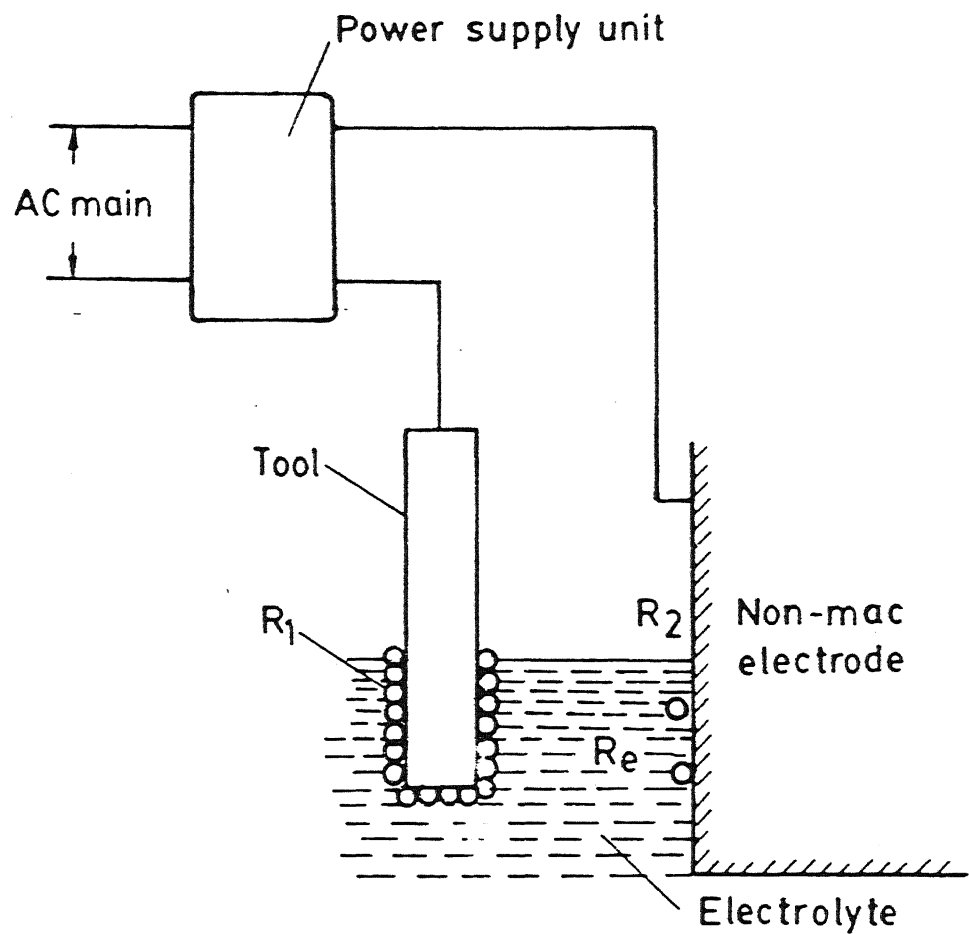


Fig.1.11 Distribution of voltage drop in an ECDM bath [Electrolyte : NaOH(35%); Tool Tool polarity : -ve ; Power supply : DC] [1]



R_e = Electrolyte path resistance

R_1 = Tool - Electrolyte interface resistance

R_2 = Non-machining electrode - electrolyte interface resistance

R_1 Fluctuates depending on voltage

Fig.1.12 Resistance in ECD (non-conductor machining) configuration [1]

holes with ECD phenomenon for machining of glass and ceramics.

Basak [2,19] has done a good number of experiments to verify the effects of different input parameters on the V-I characteristics of an electrochemical discharge cell as shown in (Fig. 1.15 -1.18.). He found that the current is proportional to the applied voltage in region 1 (Refer Fig. 1.15). Then vapour density increases and at the critical point C switching action between the electrode and the electrolyte occurs. An intermittent and irregular switching action causes the transition at region 3. Regular switching chops off the current at small intervals, so the RMS value of the current at the end of the region 3 is considerably low. The area of contact between the tool and the electrolyte is the guiding feature on current and voltage (Fig. 1.16-1.17). He also found that [Fig. (1.18)] the power consumption at the critical condition ($V_c \times I_c$) remains constant and independent of the concentration.

16.2 REVIEW OF ECDW

Only one researcher [1] seems to have made some investigation into microwelding using ECD phenomena. He has done some preliminary experiments to find out the effect of electric potential and the concentration of electrolyte (Fig. 1.13) on microwelding. His set up is designed as shown in [Fig.

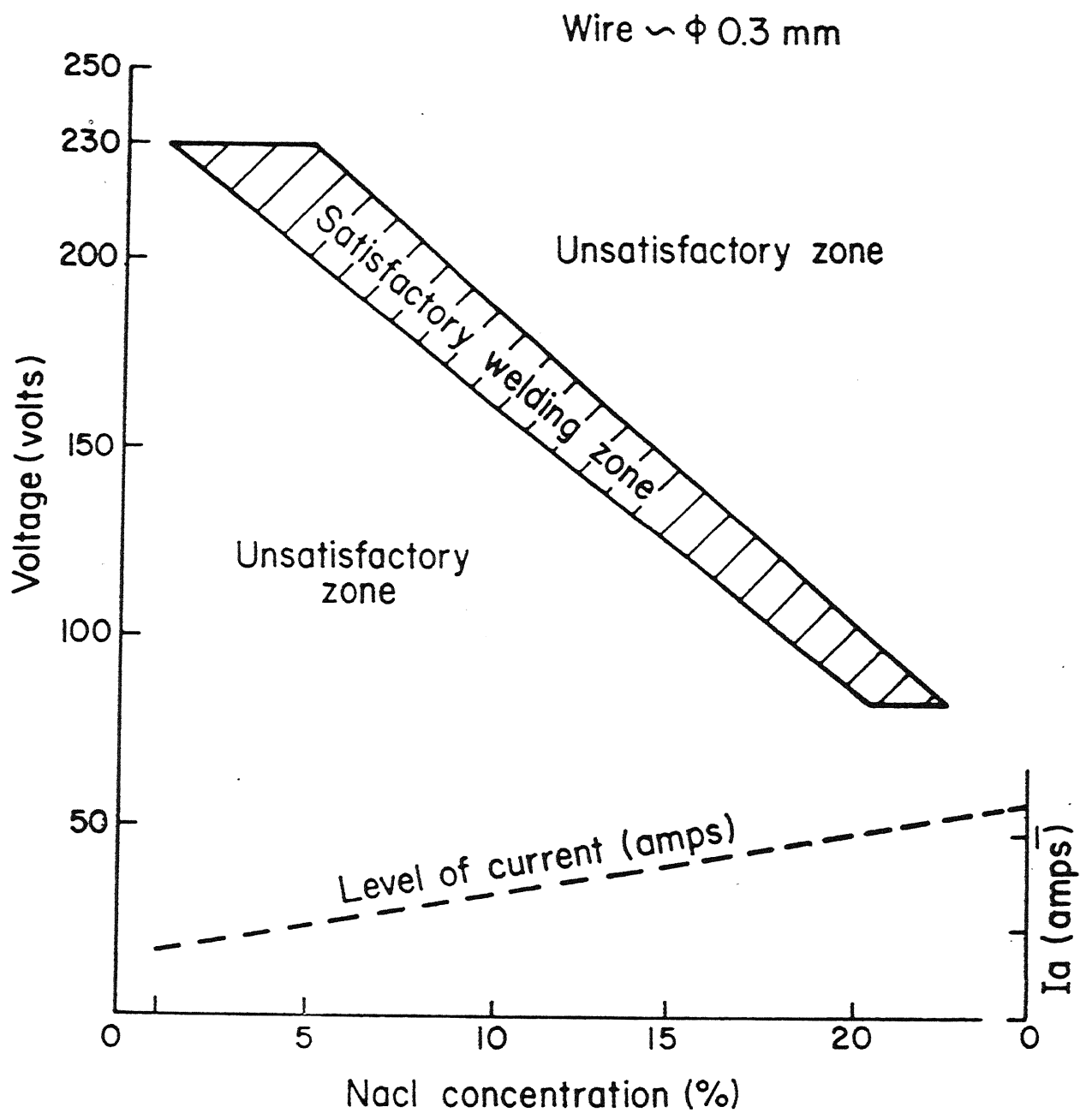


Fig.1.13 Voltage vs. electrolyte concentration in micro-welding [1].

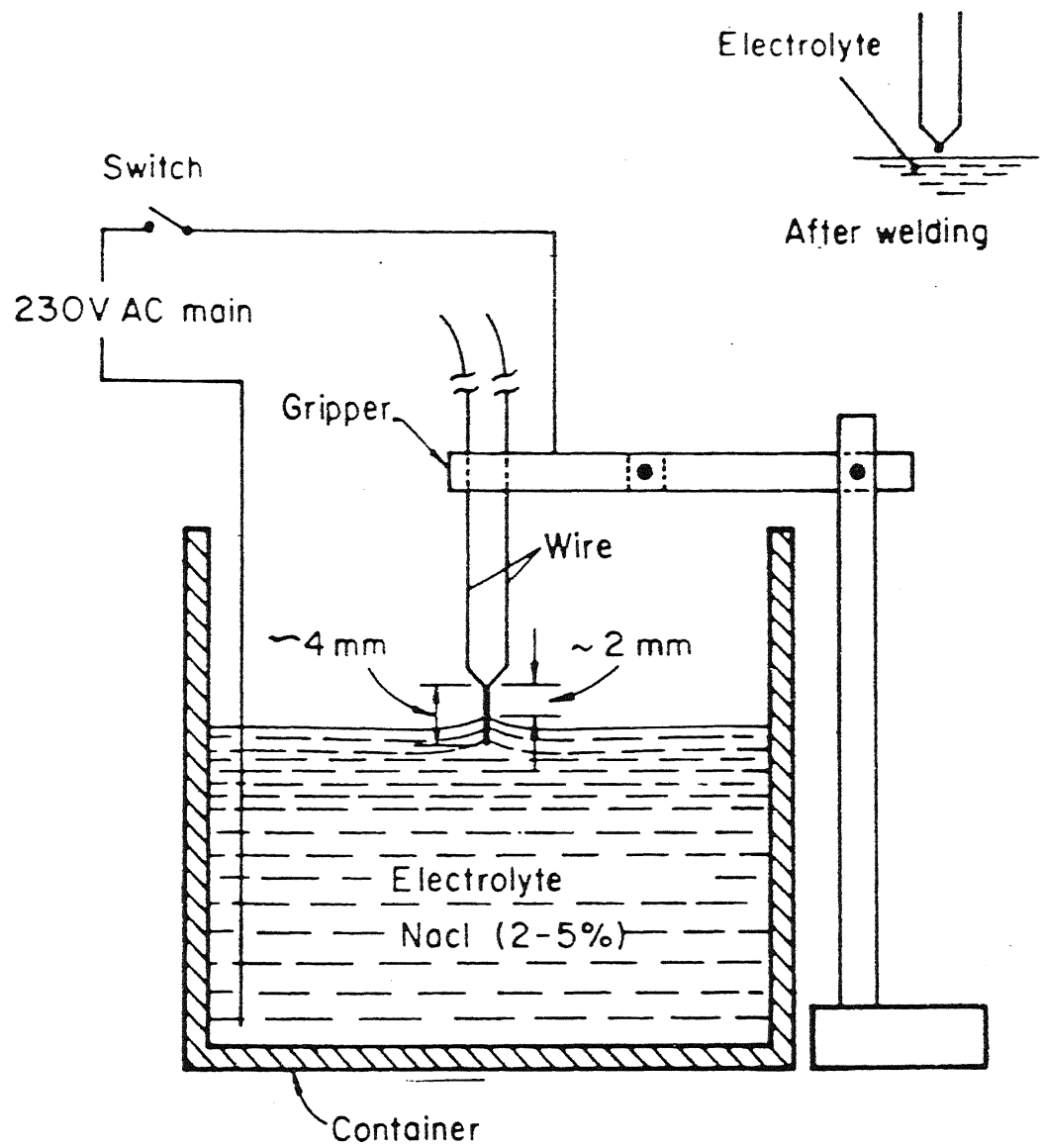
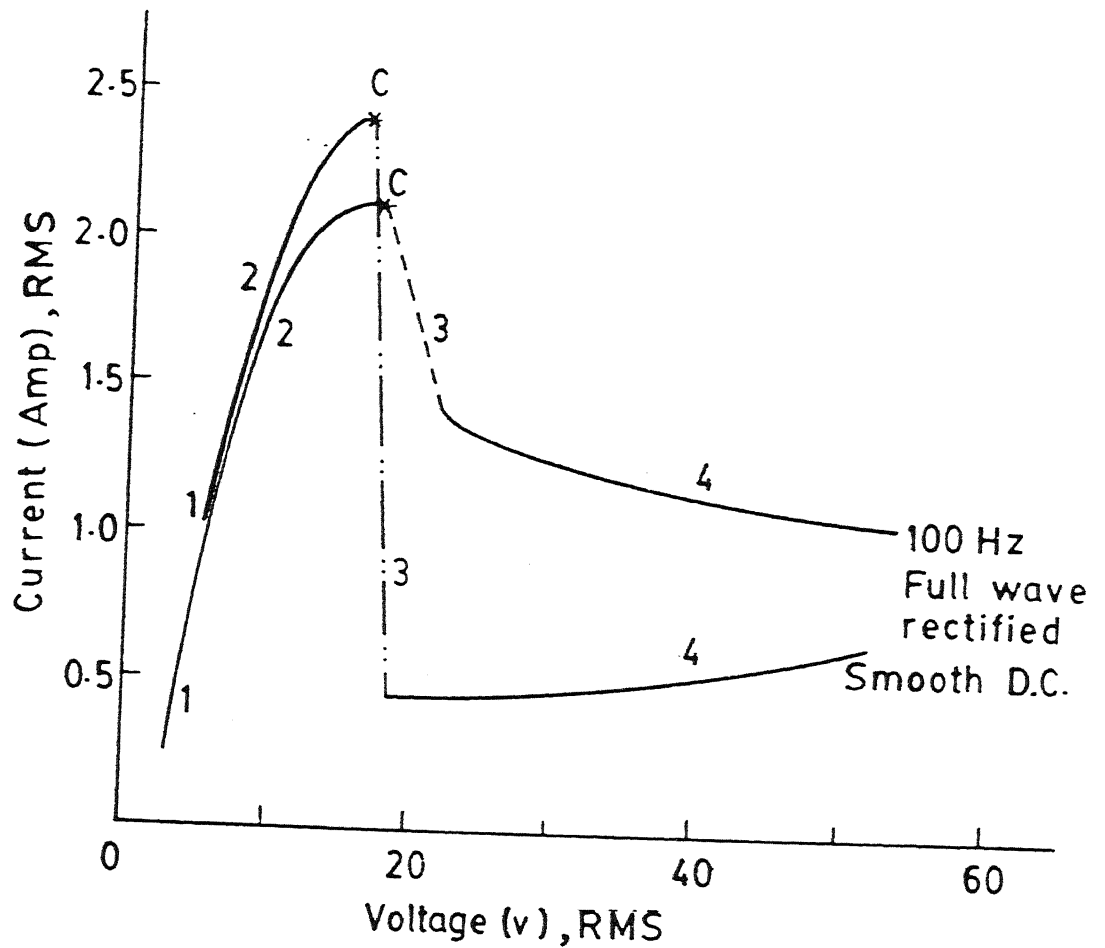
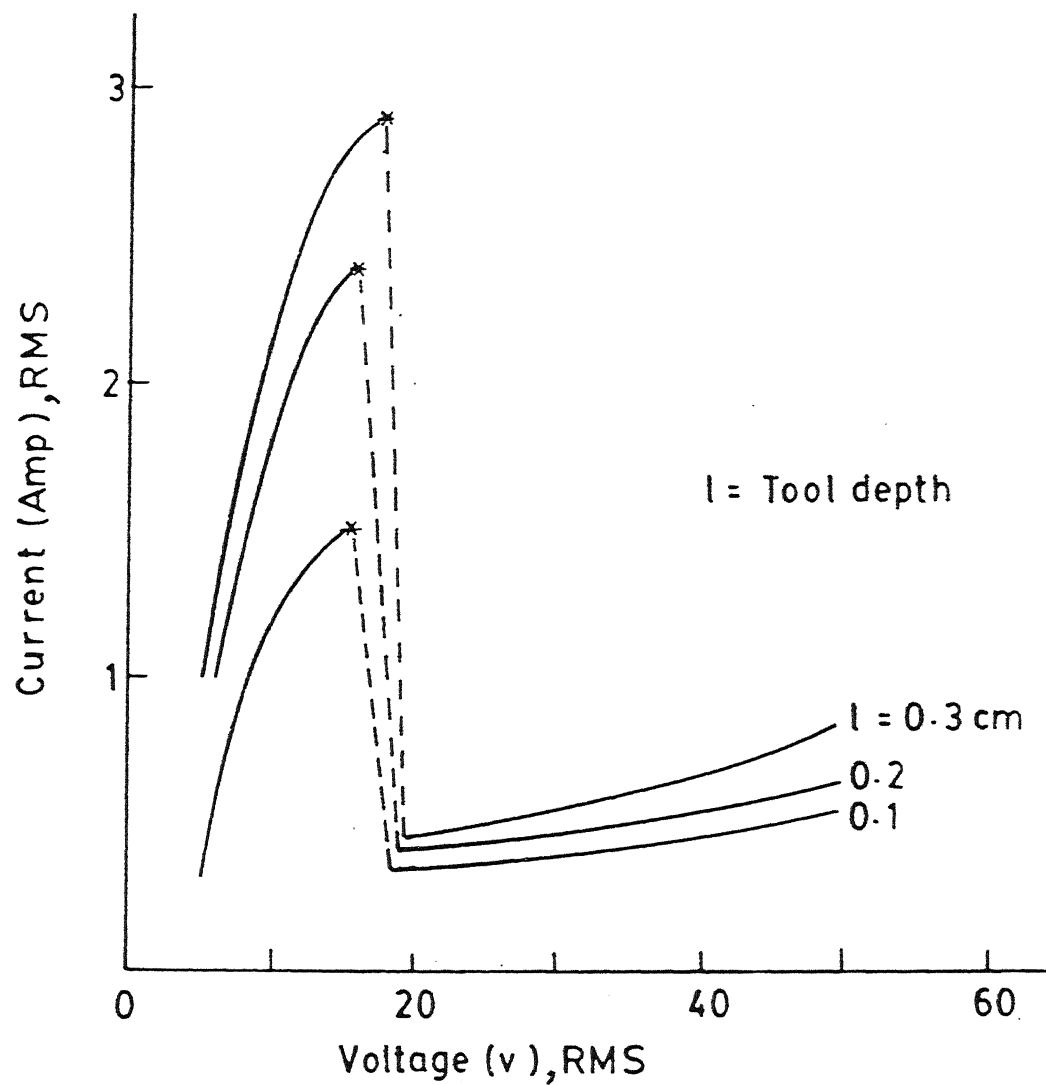


Fig.1.14 Schematics of micro-welding set-up [1]



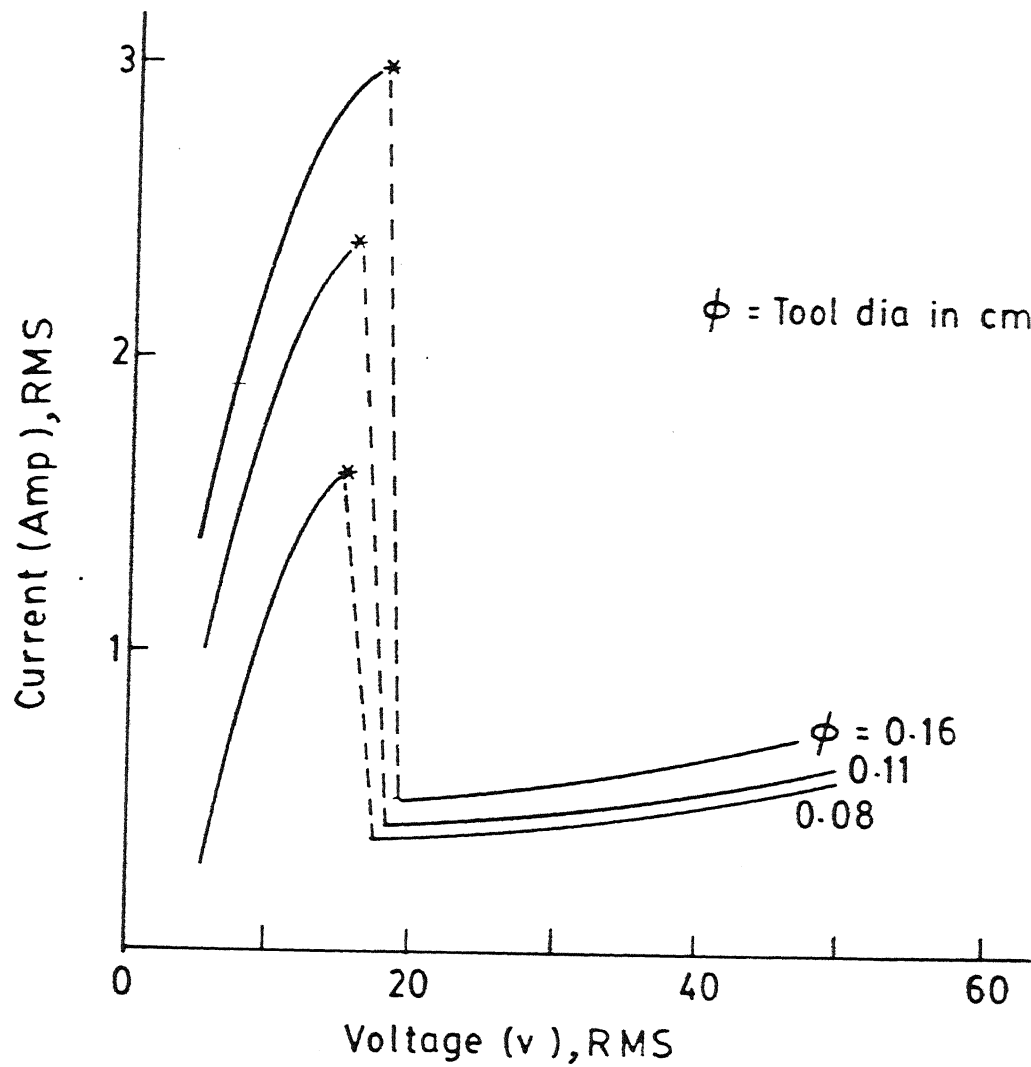
Electrolyte : 40% KOH ; Tool dia : 0.11 cm ;
Depth in electrolyte : 0.2 cm

Fig.1.15 V-I Characteristic for different type of power supply [2].



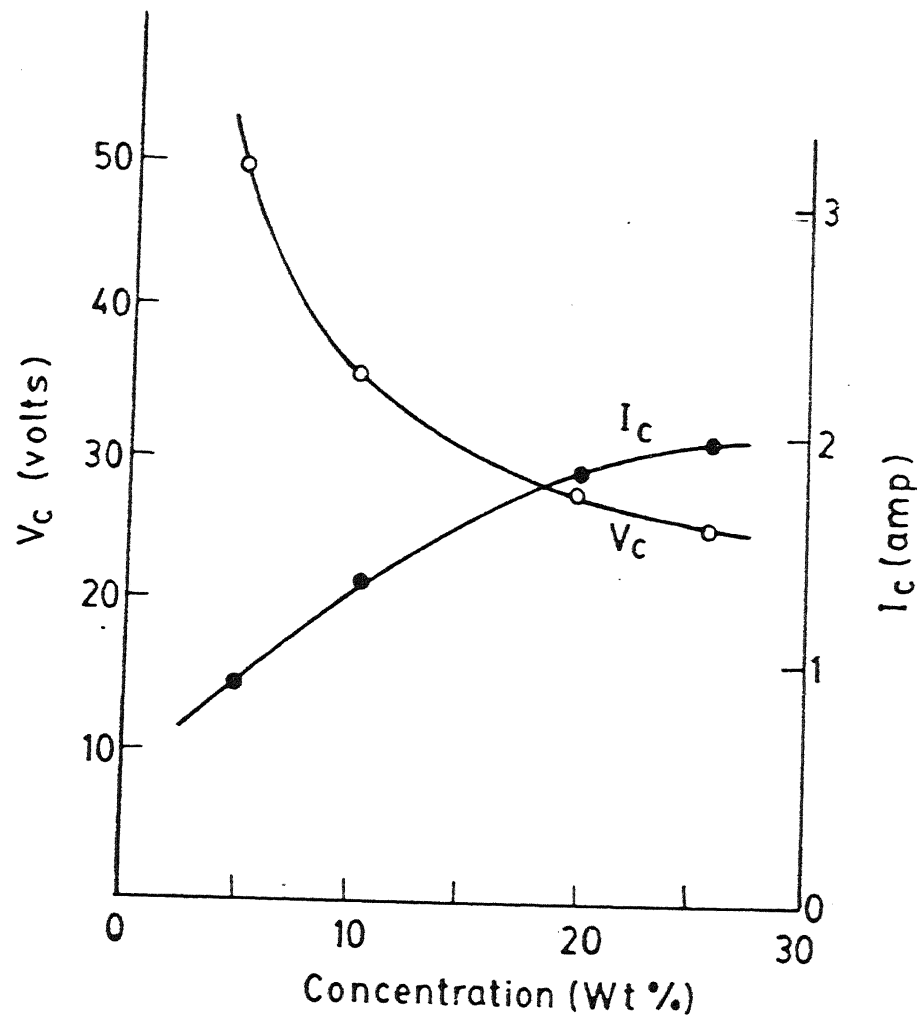
Electrolyte : 40 % KOH ; Tool diameter : 0.11 cm ;
Power supply : Smooth D.C.

Fig.1.16 V-I Characteristic for different tool depth [2].



Electrolyte : 40 % KOH ; Power supply : Smooth D.C. ;
 Depth in electrolyte : 0.2 cm

Fig.1.17 V-I Characteristic for different tool diameter
 [2]



Tool dia = 0.11 cm ; Tool depth = 0.2 cm ;
Electrolyte = NaCl ; Smooth D.C.

Fig.1.18 Critical voltage and current at different concentration (NaCl)[2]

1.14]. He conducted limited experiments using one wire size only.

1.7 OBJECTIVE AND SCOPE OF THE PRESENT WORK

The literature survey, specially the investigations of Basak, indicates that the mechanism of spark initiation i.e. the ECD phenomenon is reasonably well understood. But the use of ECD for microwelding has not been studied in details. So the main objectives of the present work are:

(1) To establish the significance of various process control parameters, i.e. voltage, current, inductance, capacitance, electrolyte concentration, depth of immersion of cathode wire and diameter of wire in microwelding of two thin wires.

(2) To obtain the optimum conditions required for attaining satisfactory thermocouple bead.

(3) To develop a simple, realistic and quantitative model capable of predicting the time required for producing the welded bead.

To study the above objectives an appropriate experimental setup is to be designed and developed. This will help in investigating the significance of the process parameters through

appropriate experiments. Full discussion is available in chapter II and III.

As has been shown in earlier works of Allesu [1] and Basak [2] the ECD phenomenon is extremely complex involving a number of interdependent phenomenon. The process of welding is also a complex process to be investigated requiring an understanding of heat transfer, melting, solidification and metallurgical aspects. Thus it is very clear that a combination of the ECD phenomenon and welding in achieving microwelding is extremely complicated to understand and analyse. Therefore the main objective will be restricted to only the gross behavioural characteristics. Besides this the experiments were restricted to a smaller number of combinations of material, electrolyte, and system parameters because of the limited availability of time and material.

The next chapter gives details of the experimental investigations.

CHAPTER II

EXPERIMENTAL INVESTIGATION OF ECD WELDING

2.1 INTRODUCTION

As already explained ECD phenomenon has led to a process which can be developed as a microwelding process (ECDW). The phenomenon of electrochemical discharge (ECD) has been investigated by previous researchers to a great extent. Their objective was mainly to use ECD phenomenon for machining of non conducting materials. So they found the significance of process control parameters suitable for machining. But in microwelding the (sparking) discharge has to be appropriate so that the twisted wires attain the melting temperature at the junction. Therefore, in the present work a set of experiments were conducted with the following purpose:

- (1) To establish the significance of various process control parameters i.e. effect of
 - (a) Voltage
 - (b) Inductance
 - (c) Capacitance
 - (d) Electrolyte concentration
 - (e) Contact area of wire electrode with electrolyte

on ECD microwelding process (ECDMW).

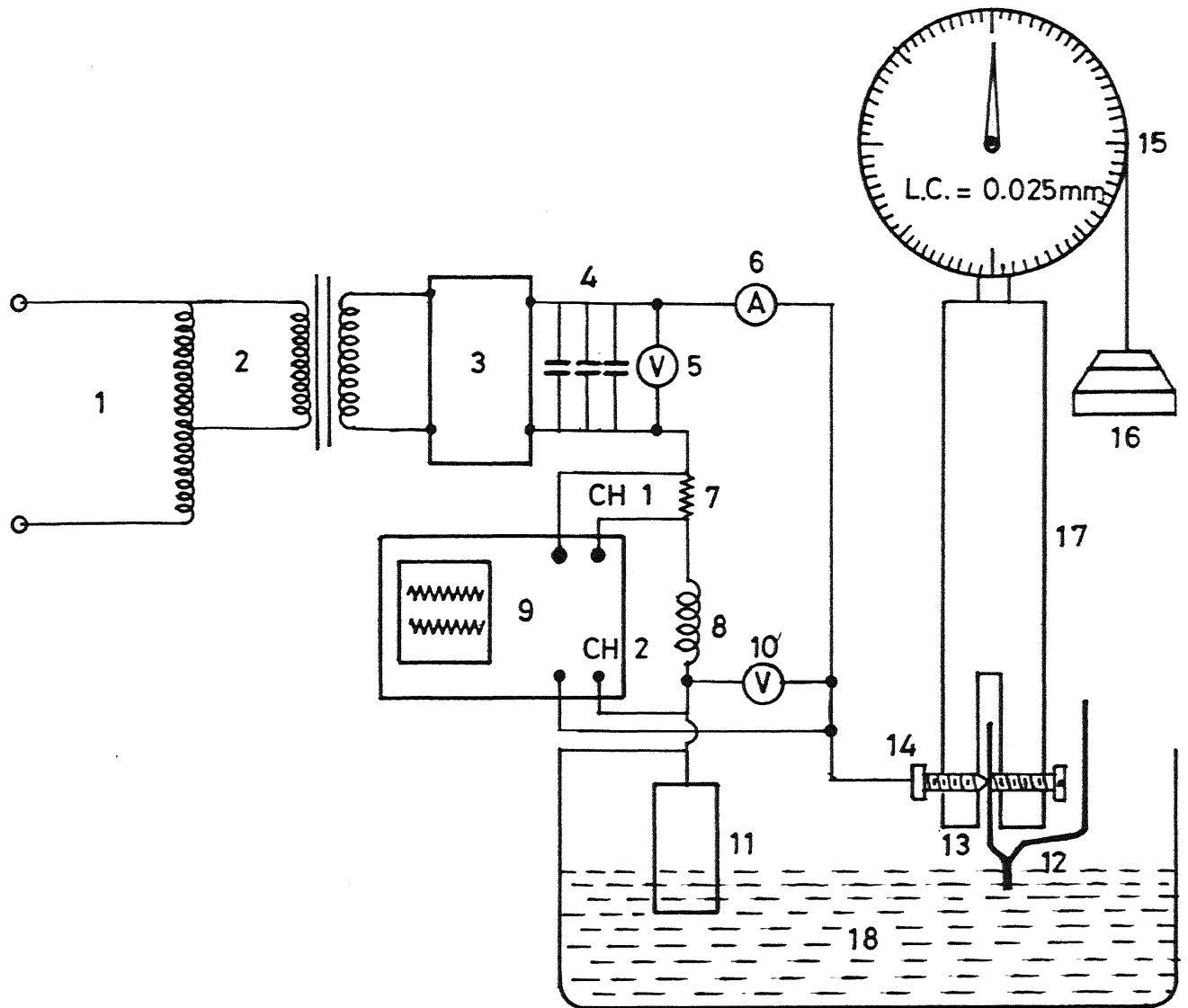
- (2) To find out the optimum condition required for obtaining a satisfactory bead by the ECD microwelding process.

An experimental set up suitable for the above said purpose was designed, fabricated and explained in next section.

2.2 DESCRIPTION OF THE EXPERIMENTAL SET UP

An experimental set up was required in which mainly the applied voltage and the depth of immersion of wire in the electrolyte would be controlled precisely. It was also necessary to record the input voltage, the corresponding input current and their wave shapes. D.C. smooth power supply was chosen as the rate of heat release is more in this case. The reason for this characteristics of ECD with DC smooth supply is explained later in a subsequent section.

The schematic view of the set up is shown in figure 2.1. The system power was taken from the A.C. mains and the input voltage was controlled by the variac and then stepped down by the transformer. Subsequently it was rectified by a bridge rectifier to 100 Hz full wave DC. Then it was filtered by connecting a capacitor bank of 1500 μ F, 350 DC and a inductance of 800mh. The two probes of the dual channel digital storage



1-Variac, 2-Stepdown transformer, 3-Bridge rectifier, 4-Capacitor bank
 5 - (RMS) Voltmeter DC. , 6- (RMS) DC Ammeter, 7- 0.1Ω Resistor, 8-Induc-
 tor, 9-Dual chanel storage oscilloscope, 10-(RMS) DC Voltmeter,
 11- Anode, 12-+ve Thermocouple wire, 13--ve Thermocouple wire, 14-Fixing
 screw , 15- Dial gauge, 16- Cöunter weight, 17- Perspex insulation tube
 18- Electrolyte bath.

Fig. 2.1 Experimental set up for ECD microwelding.

oscilloscope [DSS 2011, KIKUUSUI, JAPAN] were connected to record and monitor the magnitude and waveshapes of voltage and corresponding current. Apart from this two standard D.C. voltmeters and an ammeter were connected to measure the R.M.S. values, respectively.

The electrolyte bath was a flat bottomed glass container of 1000ml capacity in which a fixed quantity of 500ml of electrolyte was used for all the experiments.

The larger electrode (anode) which helps in completing the circuit was made from a stainless steel bar of 6mm diameter. The dissolution rate of stainless steel is comparatively low than any other electrode material. The larger electrode was made anode because of anodic dissolution. Again it was found that though sparking occurs at anode (when smaller wire electrode considered as anode) but there is no melting whatever be the applied voltage. The larger electrode was always dipped in the electrolyte to a constant depth of 10mm to avoid quick anodic dissolution. The distance between the larger electrode and twisted wire was always maintained at 40mm. This distance was chosen to maintain consistency in results. It was also found that the distance variation between two electrodes does not affect the process parameters.

The depth of the twisted wire was maintained exactly 2mm

in the electrolyte. This 2mm depth was selected on the basis of the earlier work done by Allesu on ECD Microwelding. He found this depth was satisfactory for a nice bead. This depth was maintained to study the significance of process parameters on ECD suitable for welding. Chromel-Alumel thermocouple wires of 0.48mm diameter were twisted in the same direction about 8 turns and the twisted length was always maintained equal to 4mm. The alumel wire was connected to the negative power supply line and was used as the cathode; whereas the positive wire was left open (Chromel wire). The larger electrode was connected to the positive terminal as anode (Figure 2.1). Gravity feed mechanism was used to control the depth of immersion of the twisted wire in the electrolyte. Counterweights of 50gms were used to achieve precise and accurate control of the depth of immersion.

2.3 ELECTROLYTE TYPE SELECTION

In all the experimentation reported in this work only one electrolyte was used, i.e., aqueous solution of NaCl electrolyte. It was chosen as NaCl electrolyte has low conductivity compared to NaOH (alkaline electrolyte). This is because the ionic concentration, available for surface conduction with NaCl is less compared to NaOH electrolyte. Most

of the heat generated by intense sparking at the bottom edge of the cathode will go to the twisted wire (cathode) with little loss to the electrolyte. So the major part of the heat will be utilized for the melting of wire. Aqueous electrolyte of different concentration were prepared by dissolving the appropriate amount of reagent in distilled water. The concentration of electrolyte changes due to electrochemical action. So for each set of experiments fresh electrolyte was prepared and used. The concentration expressed in percentage weight, indicates the weight of the reagent dissolved for 100ml of water to prepare the aqueous electrolyte.

2.4 THERMOCOUPLE WIRE MATERIALS AND SIZES

For microwelding wires of different materials (some being commonly recommended for making thermocouples) and of different diameters were tested. Copper wires of different diameter were also used for microwelding. The composition of various wires alongwith their properties are tabulated in Table 2.1.

TABLE 2.1
Thermophysical Properties of Wire materials

Metal or Alloys	Melting point °C	Density g/cm ³	Thermal conducti- vity k cal/s cm ⁰ c	Thermal diffusi- vity $\alpha = k/\rho c$ cm/s	Surface tension (mN m ⁻¹)
Chromel (+ve) (90% Ni + 10% or)	1430	8.73	0.325	0.338	1770.2
Alumel (-ve) 95% Ni-2% Mn-2% Al-1%	1400	8.60	0.318	0.378	1750.5
Copper (+ve) 99.98% pure	1083	8.93	0.931	1.14	1303
Constantan (-ve) 55% Cu + 45% Ni	1270	8.86	0.051	0.06	1517
Platinum (-ve) 99.999% pure	1769	21.45	0.175	0.25	2000
Pt-Rh(+ve) (10% Rh+90% Pt)	1830	19.95	0.168	0.23	1798

2.5 EFFECT OF ELECTROLYTE CONCENTRATION

The electrolyte concentration was varied to find out its effect on (i) Critical voltage V_c (The voltage when discharge occurs), (ii) Electric potential when melting starts, (iii) Critical current (when discharge starts) I_c , (iv) The RMS current I_m , when wire melting starts. In these experiments Chromel-Alumel thermocouple wires of 0.48mm diameter was used. Figure 2.2 shows the variation of V_c and V_m with electrolyte concentration by weight. Similarly Fig. 2.3 shows the variation I_c and I_m with electrolyte concentration.

It can be seen from the (Fig. 2.3a) that when concentration was between (18-27%), there was little variation both in V_c and V values. The same thing happened for I_c and I_m also in that concentration range. As a result, net power consumption remained constant, irrespective of the concentration variation in the range of 18-27%.

The reason for it can be explained as follows. Discharge behaviour can be considered to be a function of concentration and the conductivity of the electrolyte. Therefore two regions can be identified (i) the concentration range where the conductivity depends on the ionic concentration and (ii) the concentration range where the conductivity depends on the ionic mobility. The former situation exists at lower concentrations

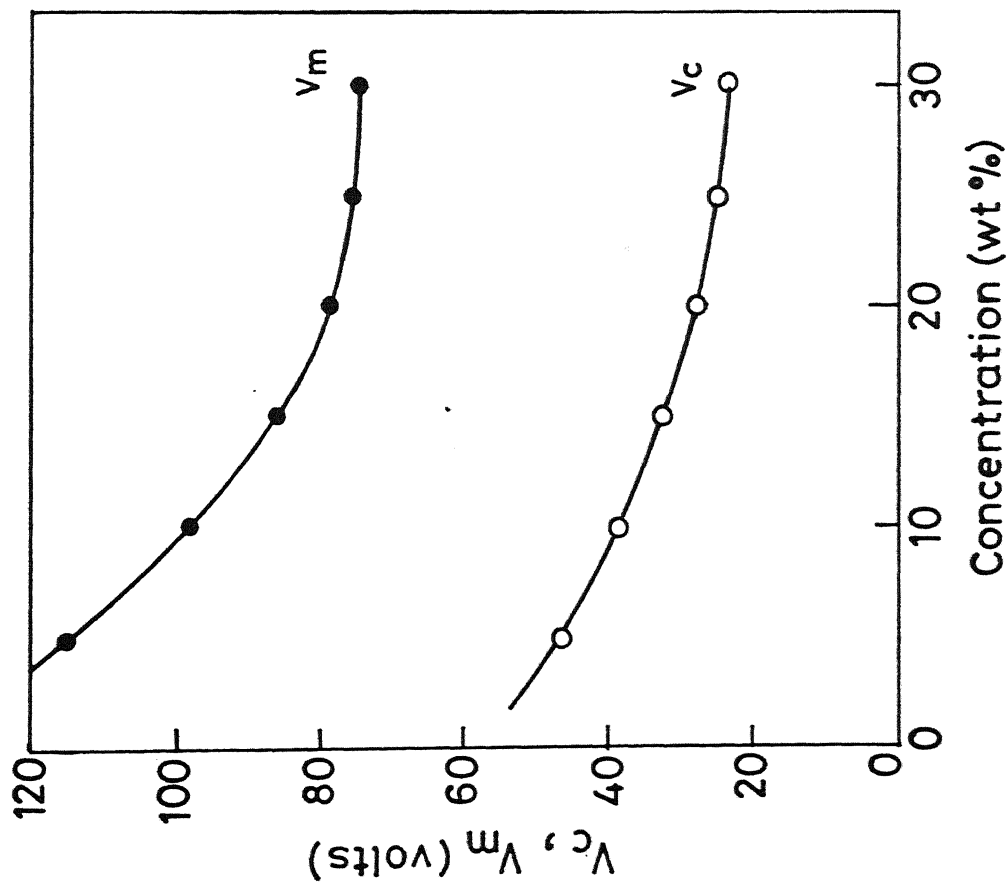


Fig.2.2 Variation of voltage parameters with electrolyte concentration

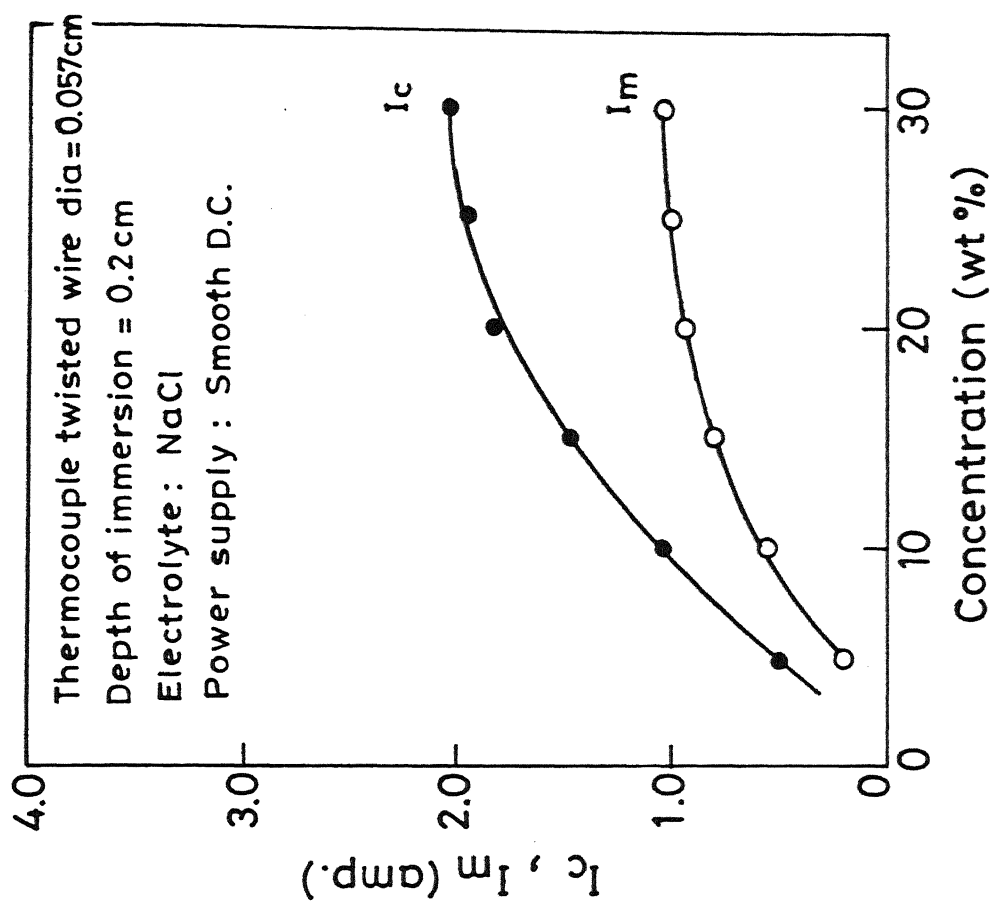


Fig.2.3 Variation of current parameters with electrolyte concentration

of the electrolyte and the latter at higher concentration. So, when the concentration was very low due to low conductivity, critical voltage and critical current was high. But as the conductivity increases alongwith concentration the ionic mobility decreases. So, applied potential and current (i.e V_c and I_c) at discharge condition as well as at melting condition (i.e V_m and I_m) vary slightly in the concentration range of 15-28%. So the remaining experiments were conducted with 25% concentration (by weight) of NaCl electrolyte.

2.6 GENERAL CHARACTERISTICS OF ECD WELDING

V-I CHARACTERISTICS

Since the intention was to obtain a satisfactory bead in minimum time, high frequency and higher intensity of discharge are the prime requirements. For this purpose voltage and current wave forms were studied with different input parameters.

(a) V-I WAVEFORM WITH INDUCTANCE IN THE CIRCUIT

Figure 2.4 shows the voltage and corresponding current waveforms as monitored and recorded in the dual channel oscilloscope. Figure 2.4 (a),(b) shows the waveform when measured between the positive and negative terminals (without electrolyte)and Fig.2.4(c),(d) shows the discharge condition

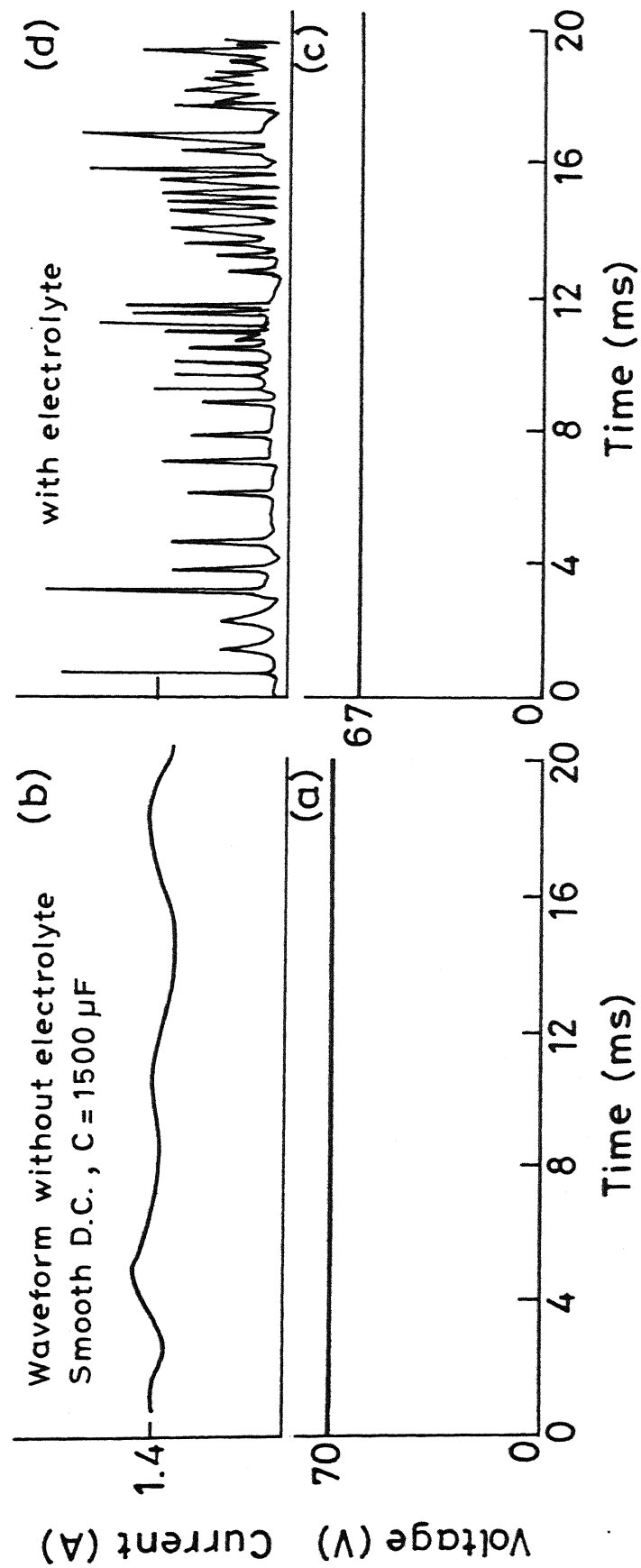


Fig.2.5 Wave shapes of voltage and current with capacitor in the circuit.

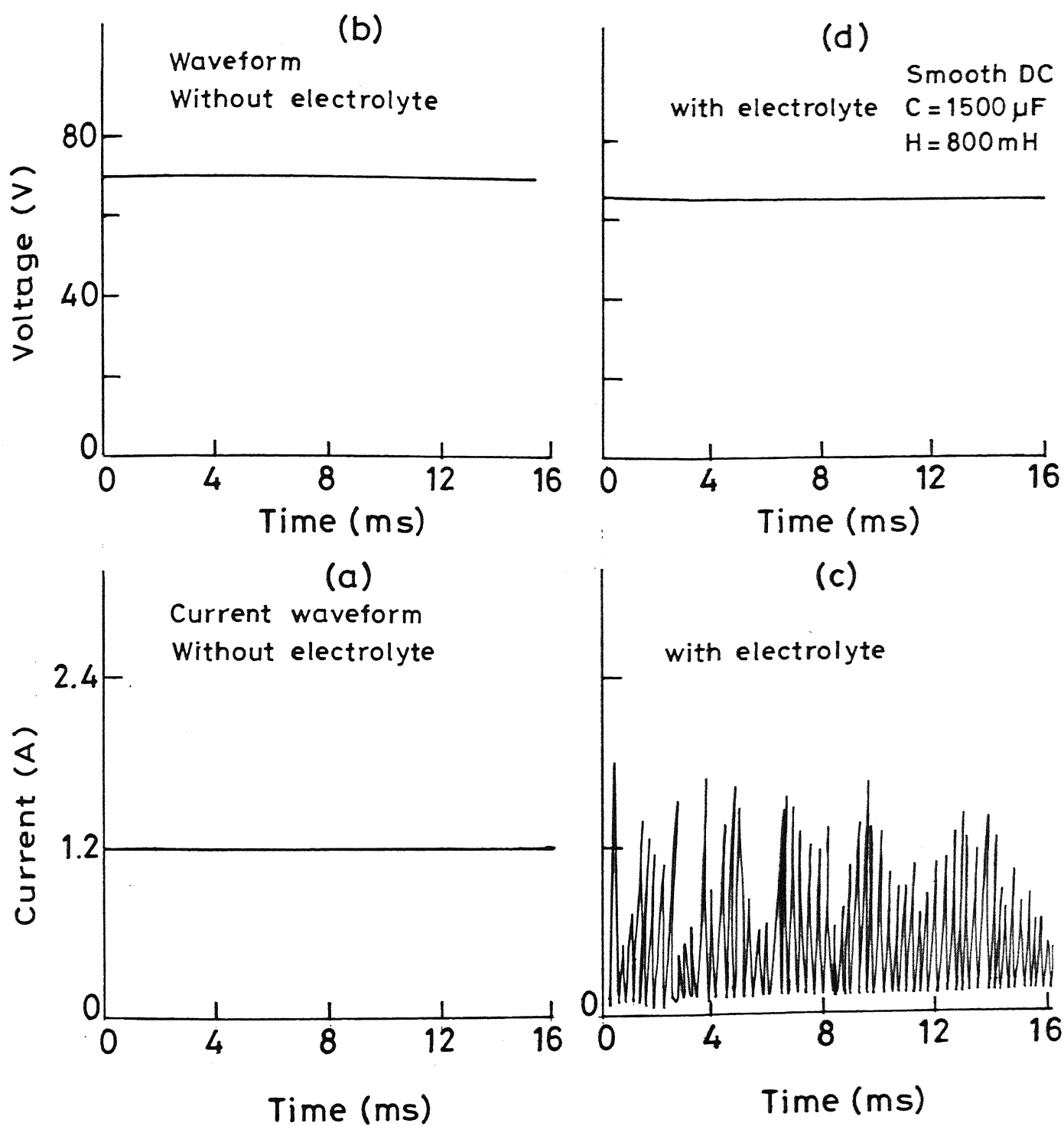


Fig.2.6 Wave shapes of voltage and current with capacitor and inductor in the circuit.

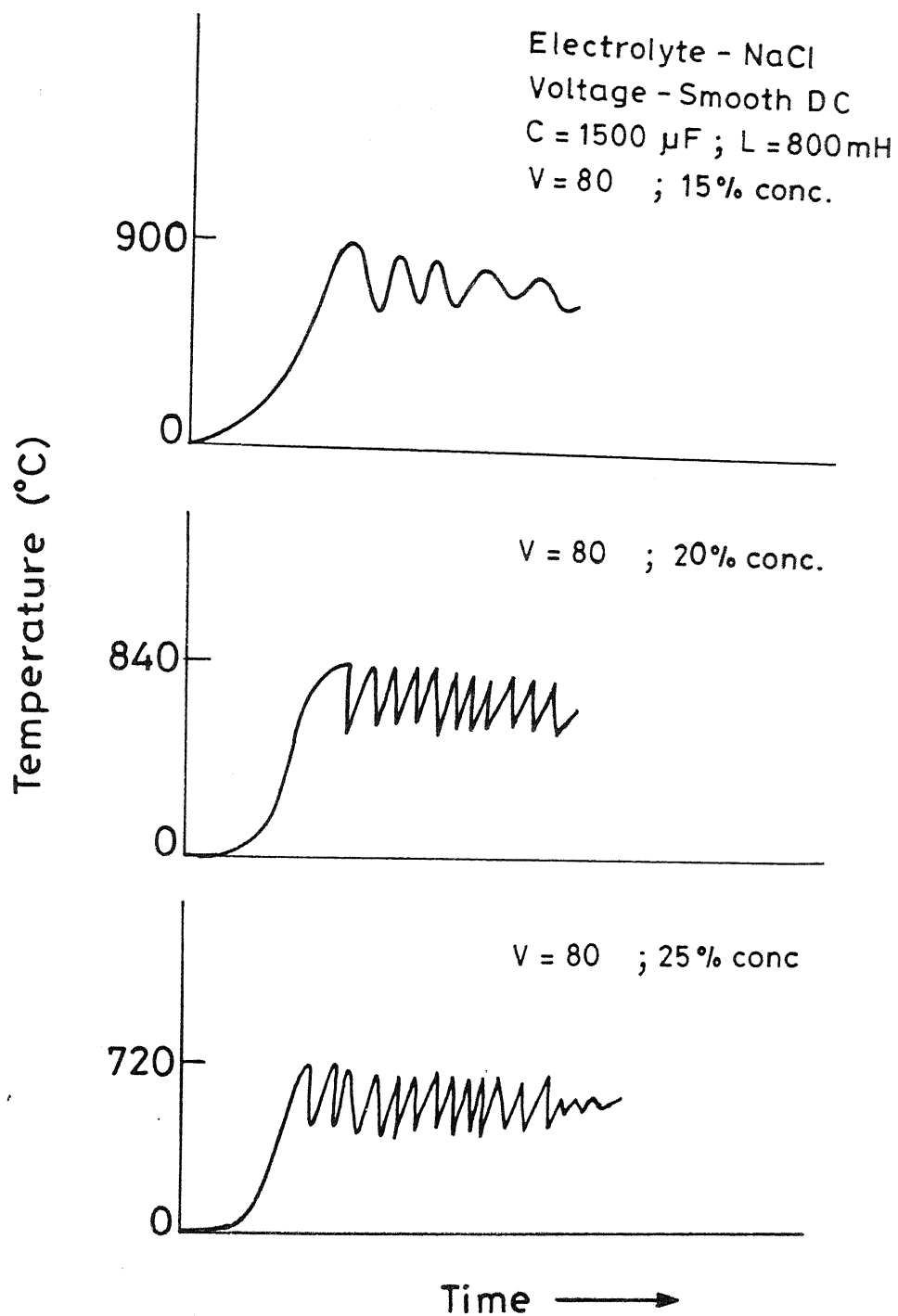


Fig. 2.6(e) Experimental pattern conforming nature of variation of temperature with time at the onset of melting.

when measured between the cathode & anode (with electrolyte medium).

(b) **V-I WAVEFORM WITH CAPACITANCE IN THE CIRCUIT** Keeping all other factors same as in the above experiment the inductor was replaced by a capacitor. In the same way the voltage and current waveforms were recorded by dual channel storage oscilloscope as shown in Fig. 2.5.

(c) **VOLTAGE-CURRENT WAVEFORM WITH BOTH INDUCTOR AND CAPACITOR IN THE CIRCUIT** Finally, both the inductor and capacitor were in the circuit and the waveforms of voltage and current were studied as shown in Fig. 2.6(b),(d) and in Fig. 2.6(a),(c). From the above three types of arrangements it was found that the current waveform had changed drastically when both capacitance and inductance were present in the circuit. It showed that the frequency of discharge and also the intensity were very high. So, insertion of both the inductance and capacitance in the circuit was found to yield microwelded at a comparatively faster rate and of good quality at the same time. The L-C circuit smoothed down the power supply that is why D.C. smooth power supply was used in the subsequent experiments. The reasons for the differences in the characteristics of the current waveforms are discussed as follows:

The power loss for a single discharge with different circuits (as explained above) is as follows:

$$0.5 (I_c - I_m)^2 L \quad (L \text{ in circuit})$$

$$0.5 (V_m - V_c)^2 C \quad (C \text{ in circuit})$$

$$0.5 [L(I_c - I_m)^2 + C(V_m - V_c)^2] \quad (L-C \text{ in circuit})$$

So it is obvious with L-C circuit that power loss for a single spark is maximum resulting in high spark energy density. At the same time both instantaneous current and the frequency of discharge are high. As a result spark energy input rate is maximum with L-C in the circuit.

2.7 EFFECT OF WIRE DIAMETER

A few sets of experiments were conducted to investigate the maximum wire diameters which could be welded properly (the wires in twisted configuration and of equal diameter). For this purpose Chromel-Alumel wires were tested with 6 different diameters ranging from 0.12mm to 1.2mm. The wires were twisted to a length of 4mm and twisting was always in the same direction. It was recommended in the OMEGA temperature measurement and control chart for thermocouple wires that a standard thermocouple bead should be thrice the diameter of the original wires, that is $D \approx 3d$, where

d = dia of the thermocouple wire

D = dia of the bead = $3d$

So, roughly the depth of immersion 'h' was estimated as follows:

$$\text{Total volume of immersion of wire} = \left(\frac{\pi}{4} \cdot d^2 \cdot h \right) \times 2$$

$$\text{Total volume of thermocouple bead} = \pi/6 D^3$$

Equating both the volumes

$$\therefore \frac{\pi}{6} D^3 = 2 \times \frac{\pi}{4} d^2 (h + D)$$

$$\therefore h \approx 6d \quad (2.1)$$

h: depth of immersion

So depending upon the wire diameter the depth of immersion was adjusted and maintained by applying appropriate counter balance-weights.

But it was found that the bead formation was never satisfactory with $h = 6d$. When the wire diameter was less (0.12mm and 0.24mm) there was bead formation. But the size of the bead was larger than thrice the wire diameter. For larger wire diameters the wires got welded and bead was formed but at the same time dropped down (detached from the parent wire). So depth of immersion was adjusted depending upon the wire diameter. Figure 2.7 shows the variation of depth with diameter, for which the standard beads ($D \approx 3d$) were obtained.

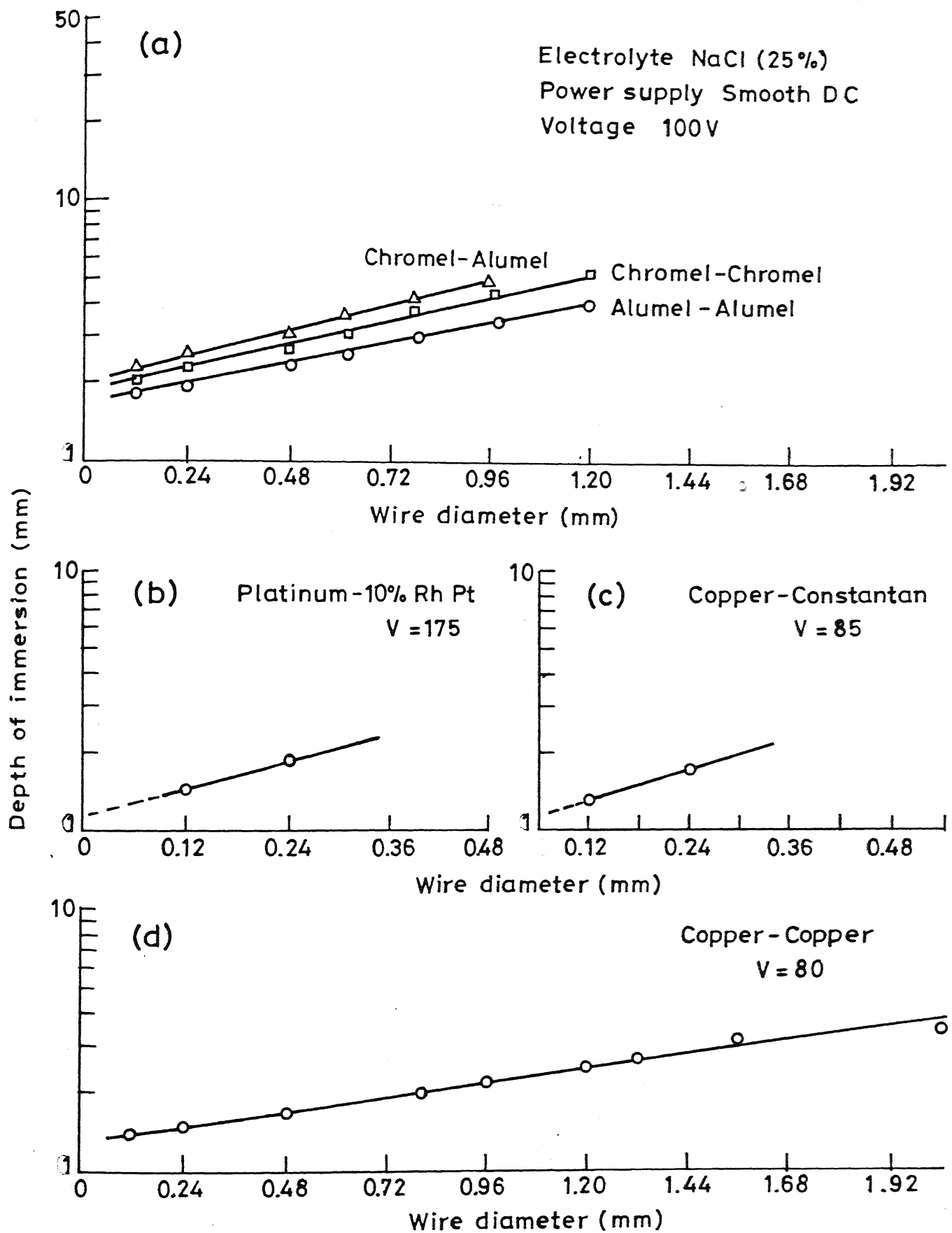


Fig. 2.7 Variation of immersed depth with wire diameter for different material composition.

2.8 EFFECT OF MATERIAL COMPOSITION ON MICROWELDING

A set of experiments were conducted maintaining different depth of immersion appropriate to wire diameter as it was done in previous experiments. Then combinations of Chromel-Chromel, Alumel-Alumel, Chromel-Alumel wires were twisted and used as the cathode. The results are shown in Fig. 2.8. It was seen that microwelding was possible for Chromel-Chromel and Alumel-Alumel pair upto 1.2mm , wire diameter. But for Chromel-Alumel the bead formation was satisfactory only upto 0.8mm wire diameter. These combinations were tested at constant applied voltage and concentration.

2.9 EFFECT OF VARIATION IN VOLTAGE ON MICROWELDING

To find out the effect of input voltage different sets of experiments were conducted, using Chromel-Alumel thermocouple wire of different diameters. The beads were examined in detail and then graded. The grading was done on the basis of

- (1) Sphericity of the bead
- (2) Smoothness of bead surface
- (3) Electrical continuity
- (4) Loss of material during bead formation

Table 2.2 shows the result of grading of beads produced. The loss of material at the end of bead formation was checked by

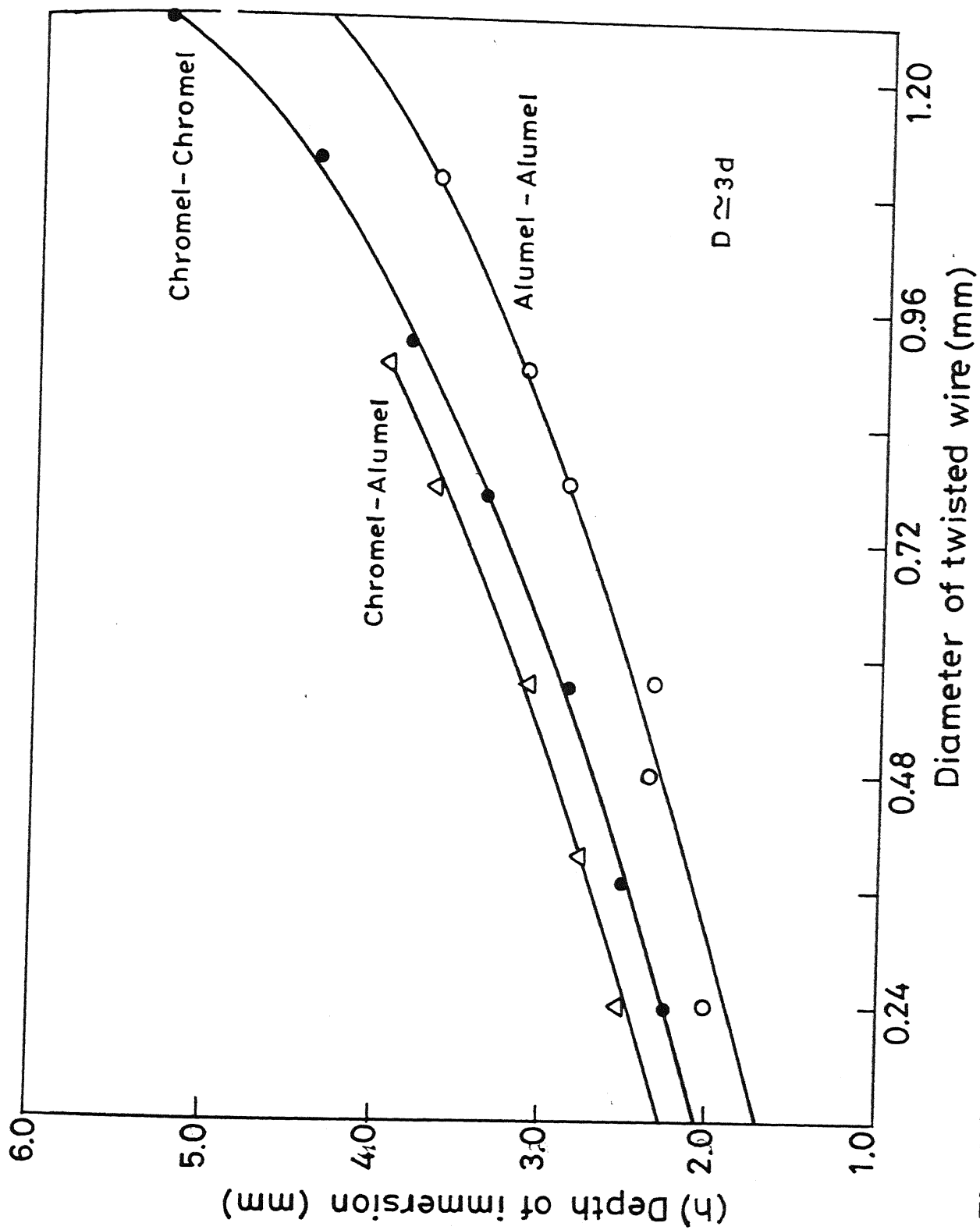


Fig. 2.8 Variation of immersed depth with wire diameter for different material composition.

weighing the specimen after and before the welding with a digital balance having 0.1mg as the least count. The loss of material vs wire diameter was plotted in Fig. 2.9 for different input voltages.

TABLE 2.2

Table showing classification of various beads obtained by microwelding

Chromel Alumel (wire)			Electrolyte - NaCl Concentration - 25% wt		
diameter in mm	0.12	0.24	0.4	0.8	1.2mm
80V					
smoothness	A	A	A	B	C
Sphericity of the bead	A	A	A	B	C
Loss of material	Nil	Nil	Nil	0.1mg	0.4mg
90 V					
Smoothness	A	A	A	B	C
Sphericity of the bead	A	A	A	B	C
Loss of material	Nil	Nil	Nil	0.3mg	0.7mg
100 V					
Smoothness	A	A	A	B	C
Sphericity of the bead	A	A	B	B	C
Loss of material	Nil	Nil	0.1	0.4mg	0.9mg

Table 2.2 shows thin wires give good beads compared to thicker ones. Even spherical nature of bead deteriorates as the

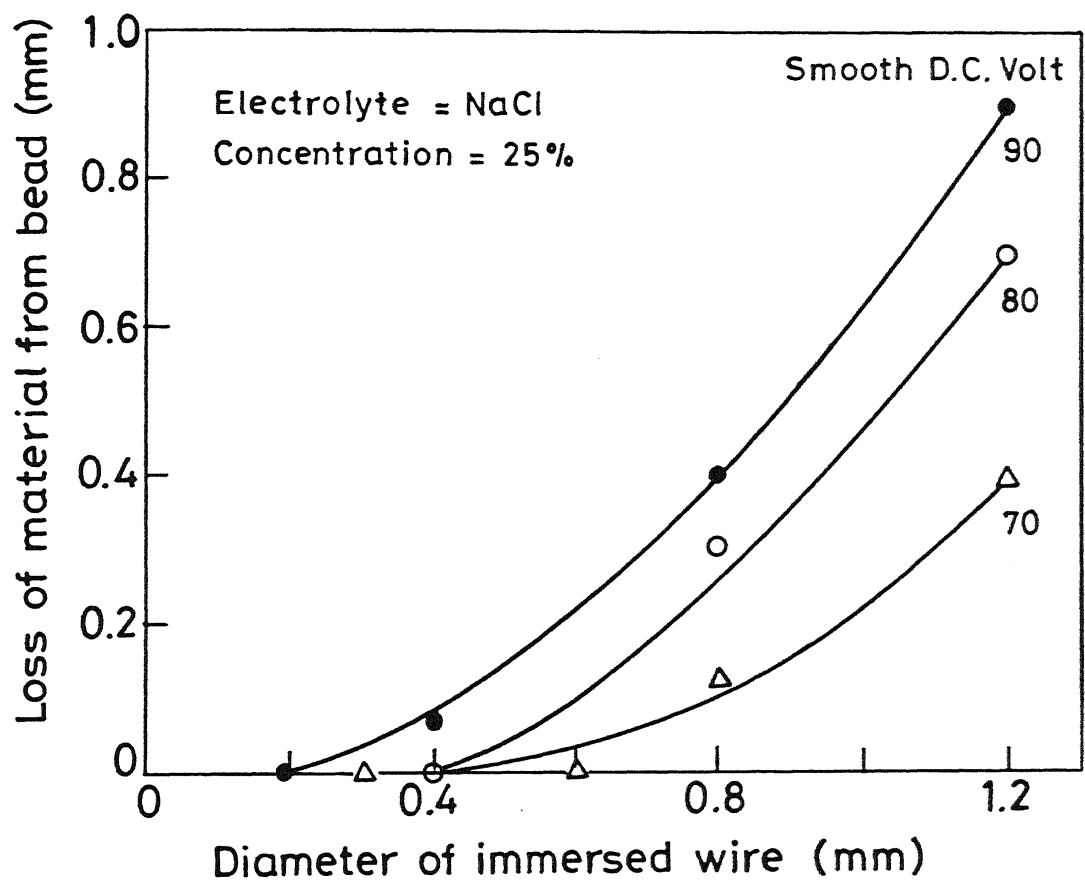


Fig.2.9 Loss of material from bead with different diameter at different voltages.

diameter increases. In case of thicker wires it was found that the beads had some microvoids due to loss of material, so the surfaces of the beads were not smooth.

2.10 MICROWELDING OF PLATINUM (10%RH)-PLATINUM, COPPER-COPPER, COPPER-CONSTANTAN WIRES

The copper wires of different diameters varying from 0.12mm to 2.4mm diameter got welded with nice beads (Fig.2.10). Though the bead was not smooth at higher diameter; but it was smooth than those with the same diameter Chromel-Alumel wire. This may be due to copper being more malleable compared to Nickel-based alloys (Chromel-Alumel) so it could withstand the shock of the spark energy density. There were minute micropores at the biggest diameter 2.1 mm.

The nature of the copper wire bead was found to be spherical in thinner dia wires and gradually the shape became oval with thicker wires whereas in case of K-type thermocouple wire the beads retained the spherical shape even with larger diameters. It is because the surface-tension of Chromel-Alumel is more compared to the surface tension of pure copper. The diameter vs depth of immersion characteristics shows that at higher depth the length (dipped) required was less and it was

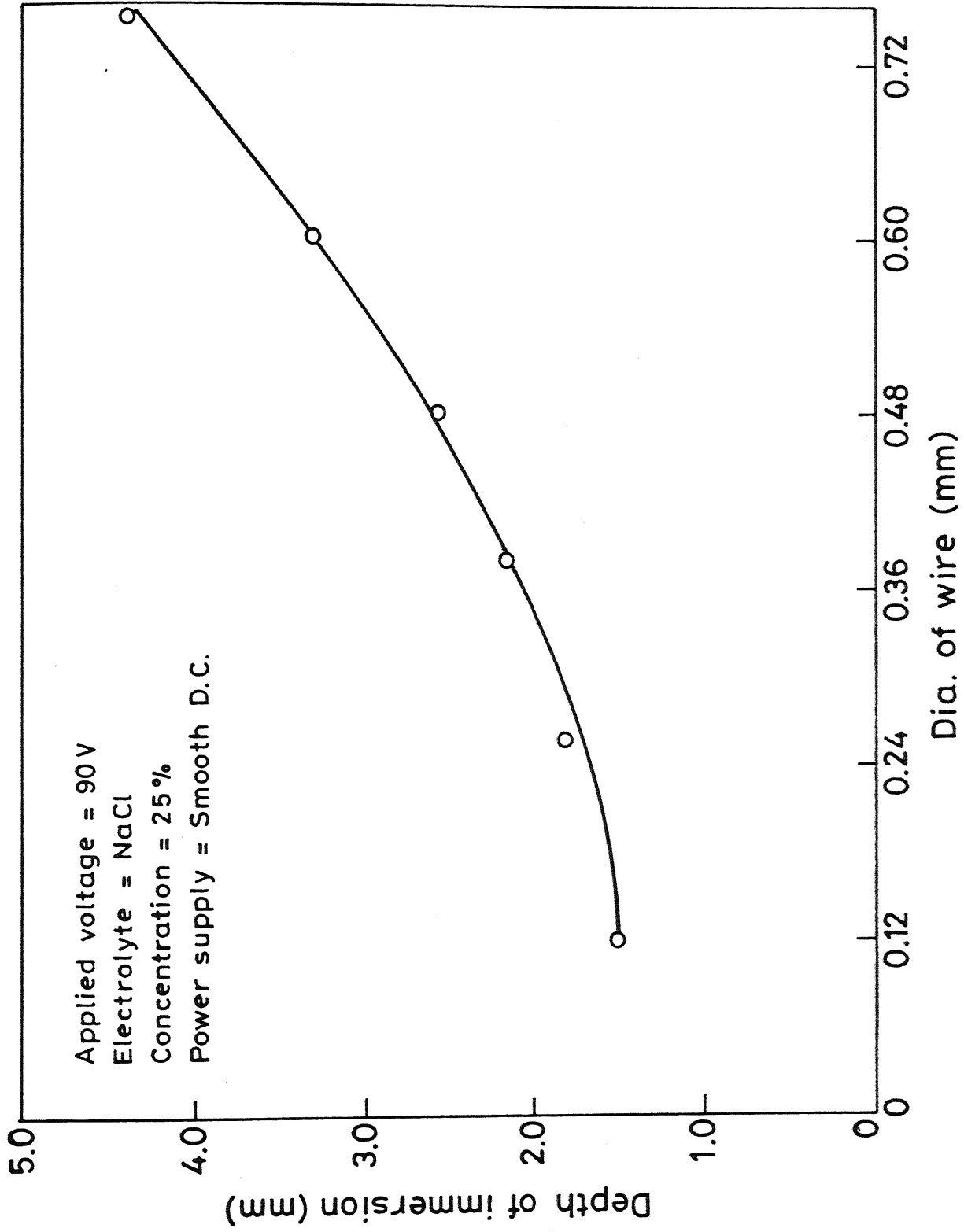


Fig.2.10 Variation in depth of immersion vs diameter of wire (Cu)

not linear. It was because the same twisted length of bigger dia wire had more volume than smaller diameter wire.

Platinum (10% Rh)-Platinum thermocouple wires of 0.12 and 0.24 diameter got welded with nice bead at around 175 voltage. Higher voltage was required because its melting temperature is quite high. The nature of variation of depth of immersion vs wire diameter is shown in Fig. 2.7. From the plots it is clear that the depth of immersion increases exponentially with the wire diameter. Thus without causing much error, a general relation between h and d can be approximately expressed in the following form: $h = h_0 e^{\lambda_0 d}$ the values of h_0 and λ_0 for different cases were estimated from Fig. 2.7 and tabulated in Table 2.3

TABLE 2.3

Metal or Alloys	λ_0	h_0
Copper-Copper	0.62	0.3
Chromel-Chromel	0.65	0.75
Alumel-Alumel	0.64	0.7
Chromel-Alumel	0.66	1.0
Copper-constantan	2.5	0.15
Platinum(10%Rh)-Pt	3.9	0.1

CENTRAL LIBRARY
111 14802

2.11 MECHANISM OF MICROWELDING

As shown in Figure 2.11 when the voltage was around 80V there was intense sparking around the bottom edge of twisted wire (Fig 2.11a). The twisted wire got melted at the outer circumference and formed a molten pool (fig 2.11(b)). Gradually the heat energy conducted towards the centre and the centre reached melting temperature (fig 2.11(c),(d)). During this period the outer molten metal zone was attached to the individual parent metal wire by surface tension force. When the centre of twisted wire (i.e. the point of contact of two wires) got melted at point A as in figure 2.11C, the entire molten pool shape became elliptical and then circular (fig 2.11(f),(g)). As the melting process continued the depth of immersion decreased and heat was conducted in upward direction also. The size of the bead increased gradually and finally the hemispherical shape became spherical when came out of electrolyte. The stages in microwelding are shown in figure 2.11.

2.12 MECHANISM OF VOID FORMATION (IN BEADS)

As found from table 2.2 there was some void formation on the bead when the diameter of wire was more. As the wire diameter was increased the depth of immersion also increased i.e. wire-electrolyte contact area became more. The average

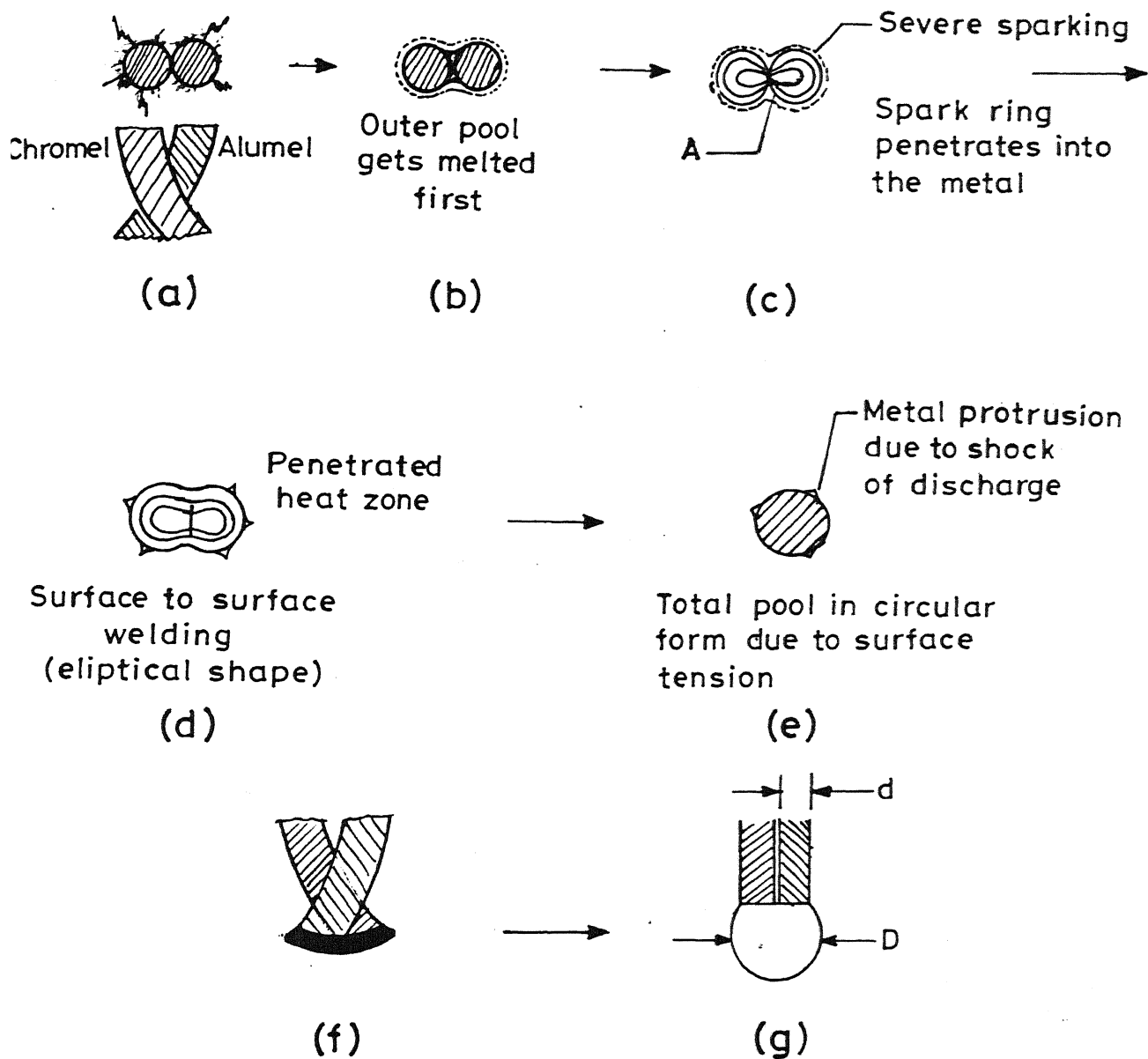


Fig.2.11 Stages in microwelding

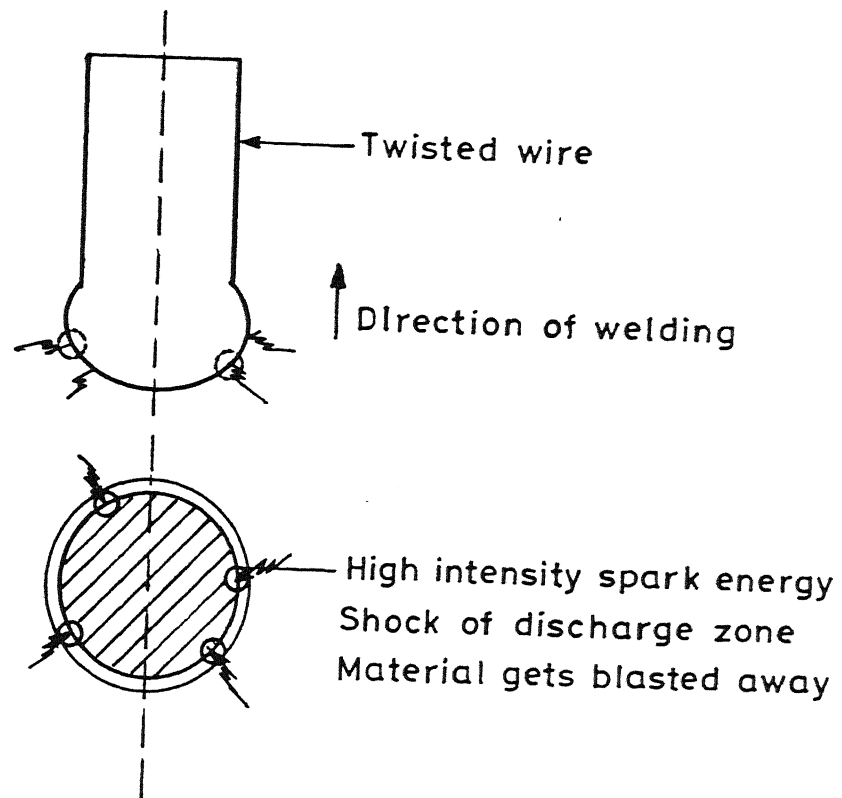


Fig.2.12 Mechanism of void formation.

current density being constant the twisted wire would draw more current and the total power loss for single discharge. $\frac{1}{2}[(I_m - I_c)^2 L + C (V_m - V_c)^2]$ would become more. i.e. the discharge intensity would increase. The higher spark energy density gave a shock of discharge to the outer molten metal pool as shown in Fig. 2.12. When the shock energy was more than the surface tension force, it blasted away some material leaving voids in the final bead. The location of void depends on random sparking position.

2.13 SATISFACTORY WELDING ZONE AS A FUNCTION OF VOLTAGE WITH D.C. SMOOTH POWER SUPPLY

Different wire diameters of various materials as already used in previous experiments were used to find out the range of voltage for satisfactory microwelding. The different concentration of electrolyte were also used. The result was then super imposed on the results obtained by Allesu [1] as shown in Fig..2.13. It shows that irrespective of wire diameter the voltage variation was within a closed range. Voltage above the range could melt the wire but the bead broke from the wire. This might be because of severe ECD at higher voltages and as a result high spark intensity occurred. So the twisted wire portion just above the electrolyte also got severely heated and broke at that point due to oxidation of the wire with

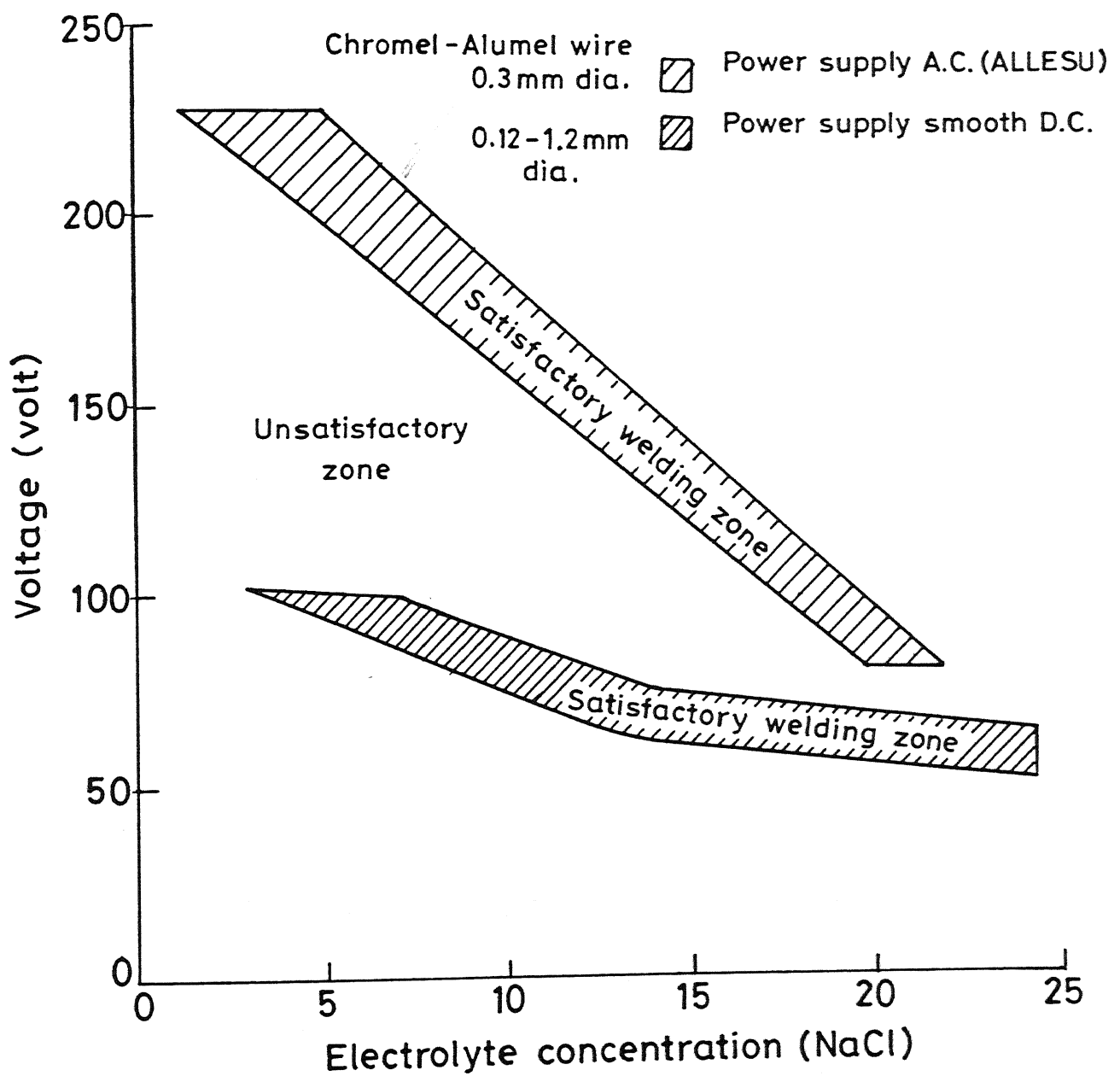


Fig. 2.13 Nature of voltage - electrolyte concentration in microwelding.

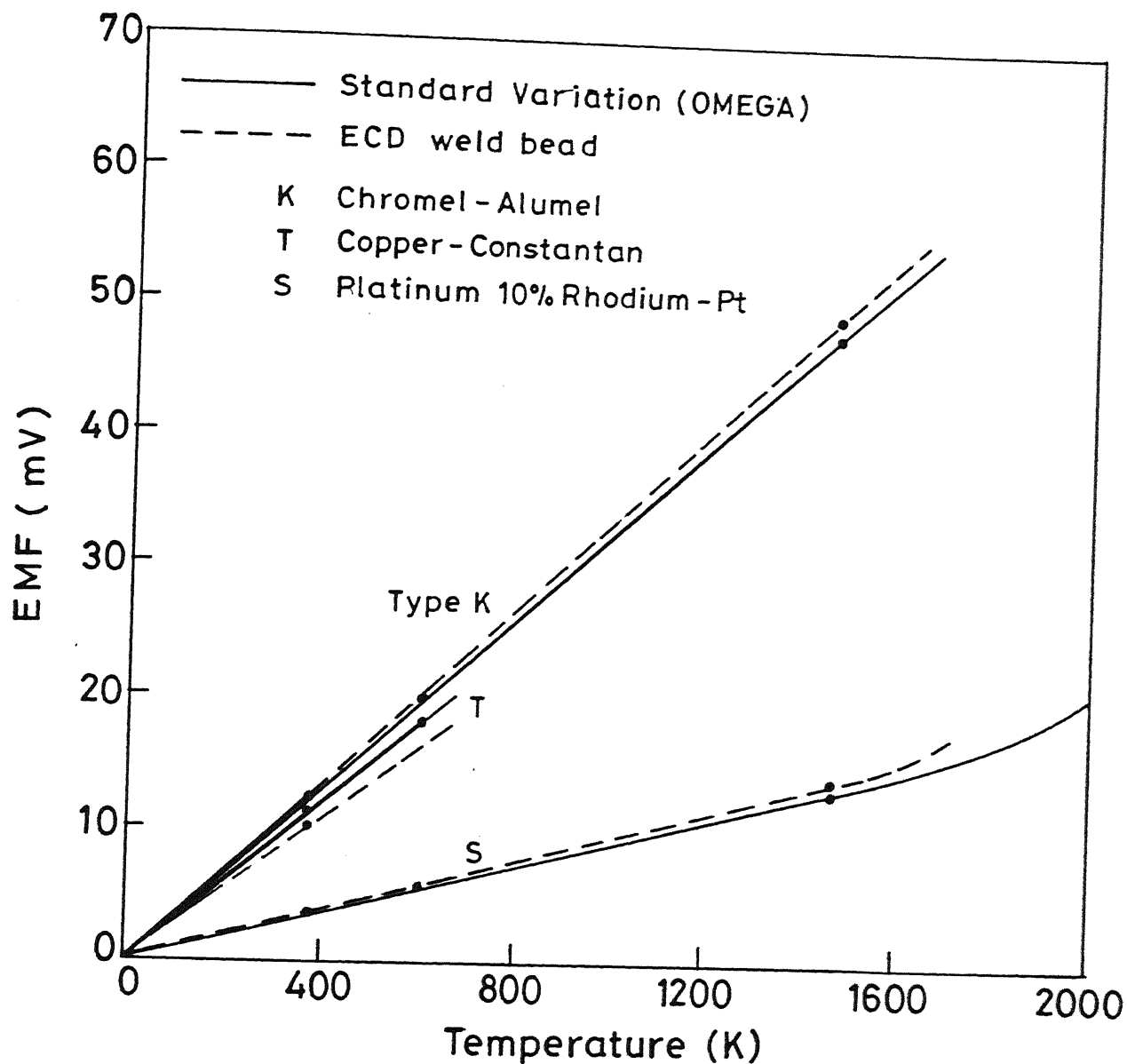


Fig.2.14 Comparison between standard temperature - milivolt calibration graph and that obtained by ECD weld bead.

atmospheric air. Below the satisfactory voltage range ECD was not intense to melt the wire.

It could be also noted that at lower concentrations voltage requirement was high because of splashing and turbulence of electrolyte which interrupts the arcing conditions. When the concentration varies from 15-27% the input voltage was almost constant with a little variation. It indicates that electrolyte of a given concentration can be used for a long time to get several beads prepared at the particular voltage. This would be of much importance in actual industrial application. From Fig. 2.13 it can be also concluded that applied potential with D.C. smooth supply was low compared to A.C. power supply. This is so because the discharge intensity was more in former case, which was explained earlier.

2.14 COMPARISON OF CALIBRATION CHART

The standard E.M.F. temperature calibration that of different electrocouple materials as prescribed OMEGA was shown in Fig.2.14. The standard beads of different thermocouple materials prepared by ECD microwelding method were to used to measure the room temperature, boiling water temperature, candle flame temperature. The e.m.f. vs temperature rise chart was prepared and then superimposed on standard e.m.f. temperature

chart (Fig.2.14). It could be seen at lower temperatures that coincided with standard calibration. And when the temperature was high the e.m.f. response of ECD welded beads slightly deviate from the standard beads. This could be due to the different bead preparation method, which might have changed the distribution of constituent method in the bead.

CHAPTER III

THERMAL ASPECTS: THEORETICAL ANALYSIS EXPERIMENTAL VERIFICATION.

3.1 INTRODUCTION:

While investigating the ECD phenomenon it was found by the previous researchers that the electrochemical discharge (sparking) takes place at the outer circumference of the cathode tool edge because the current density is maximum here as shown in Fig.1.8. As the input voltage increases the frequency of discharge and the intensity of spark also increase. As a result the sparking zone becomes an annular heat source formed around the cathode wire electrode edge. The remaining portion of the immersed wire electrode is assumed to be insulated as described in the previous chapters.

In ECDW the immersed twisted wire has to attain the melting temperature of the corresponding materials so that welding would be possible. When the bead centre attains the melting temperature we assume the welding to be achieved. Keeping this in view a simplified theoretical model was proposed which would predict

- (i) the temperature at the centre of the twisted wire assumed to be a solid cylinder,
- (ii) time taken for the centre to reach the melting temperature,
- (iii) the nature of variation of temperature with time,

(iv) the effect of the following process control parameters:

- (a) properties of the wire material
- (b) dimension of wire (diameter, immersed depth of twisted wire immersed, total length of twisted portion)
- (c) type of electrolyte
- (d) electrolyte concentration
- (e) nature of power supply
- (f) input voltage.

3.2 THEORETICAL MODEL: Estimation of temperature as a function of time.

3.2.1 ASSUMPTIONS: Because of the complexity of the problem it is essential to make a few assumption so that a theoretical model is possible. These assumption are as follows:

- (i) The twisted wire was considered as a wire having equivalent uniform diameter ' D_o ' which was taken to be

$$D_o = \sqrt{2}d$$

where d = diameter of individual wire.

- (ii) It was considered as a homogeneous semi-infinite cylinder insulated from the bottom and around the immersed circumference; except near the edges as

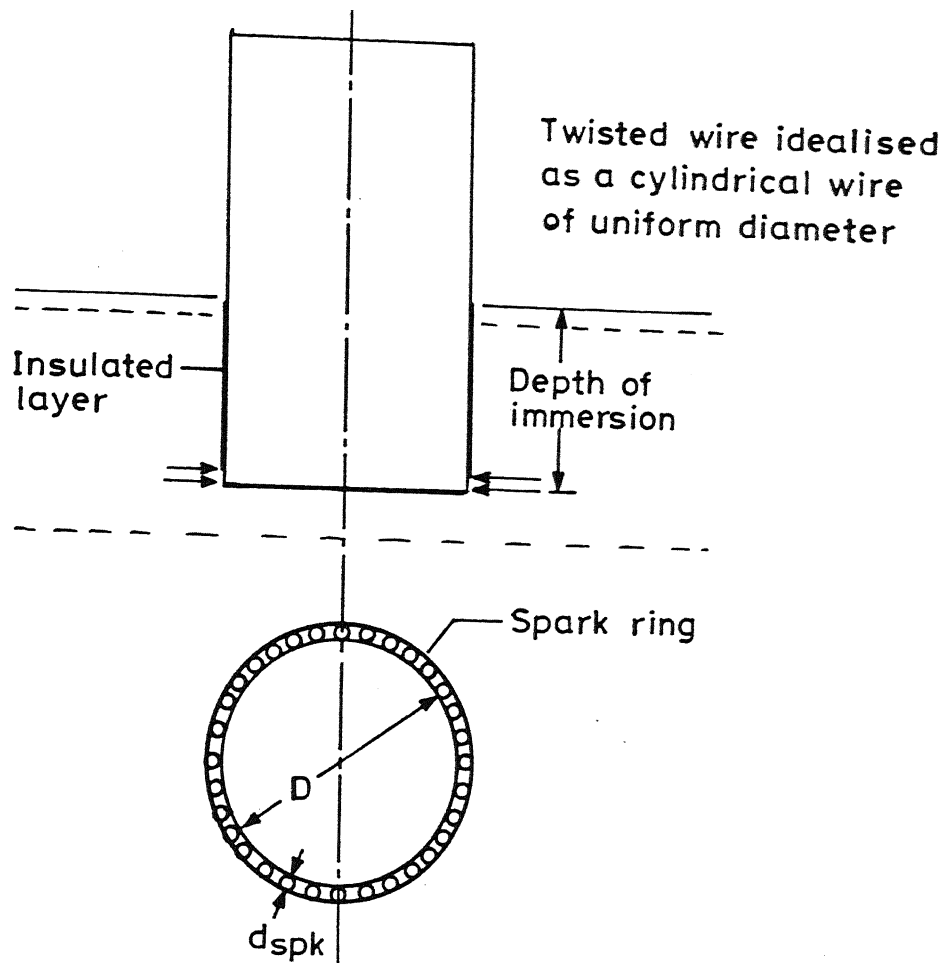


Fig. 3.1 Circular heat source around the bottom edge of the electrode.

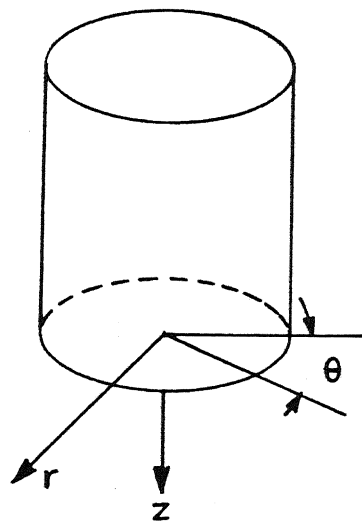


Fig. 3.2 Representation of wire in cylindrical co-ordinate system.

shown in Fig.3.1.

- (iii) The heat generation rate is constant i.e. spark energy density and the frequency of sparking around the bottom edge circumference of cathod wire remaining constant.
- (iv) Electrolyte concentration remains constant when the process continues.
- (v) The thermophysical properties of the wire material are identical for the solid and the liquid phase of metal.
- (vi) All the heat is conducted by the wire cathode without any transfer to the electrolyte.

3.2.2 PROBLEM FORMULATION

The twisted wire configuration was considered as semi-infinite cylinder with the heat source around the bottom edge circumference having equivalent diameter as ' D '. The depth of immersion was ' h ' as shown in Fig.3.1. At the beginning the heat source was considered at a point (single spark) around the circumference $(a, 0, 0)$. Then the problem was evaluated for a (circumferential) constant ring heat source. The coordinate system used is shown in Fig.3.1 with respect to the immersed wire.

For continuous constant source along the circumference of wire when $r=a$, the above equation 3.3 had to be integrated with respect to θ in the interval $0-2\pi$.

Now the temperature at $T(0,0,0,t)$ due to a line (ring) heat source of strength $\frac{Qd\tau}{\rho c}$ was evaluated as

$$T_o(0,0,0,t) = \frac{Q}{\rho c} \int_0^{2\pi} \int_0^t \frac{t}{2\pi a^2 \sqrt{\pi \alpha (t-\tau)}} \left[\sum_{\lambda} \frac{e^{-\alpha \lambda^2 (t-\tau)} J_o(\lambda a)}{J_o^2(\lambda a)} + 1 \right] d\theta' d\tau$$

The final solution would be as follows:-

$$T_o(0,0,0,t) = \sum_{\lambda} \frac{Q}{\lambda a^2 \rho c \alpha J_o(\lambda a) \lambda} \left[\operatorname{erf} \lambda \sqrt{\alpha t} + \sqrt{\alpha t} \right] \quad (3.5)$$

The actual temperature would be

$$T(t) = \sum_{\lambda} \frac{Q}{\lambda a^2 k J_o(\lambda a) \lambda} \left[\operatorname{erf} \lambda \sqrt{\alpha t} + \lambda \sqrt{\alpha t} \right] + 298^\circ \text{K (Ambient temperature)} \quad (3.6)$$

where

α = Thermal diffusivity, in cm^2/s ,

k = Thermal conductivity, in $\text{J/s-cm-}^\circ\text{C}$,

Q = Heat input, in cal/s ,

a = radius of the equivalent, wire = $D_o/2$ in mm,

h = depth of immersion.

$T(t)$ = actual temperature in $^\circ\text{K}$.

3.2.3 NUMERICAL EVALUATION OF THE SOLUTION

Equation 3.6 indicates that the melting temperature of the wire is a function of the wire diameter, rate of heat generation and thermophysical properties of the wire material. The heat generation rate is again a function of the type and concentration of the electrolyte, effective area of wire (cathode) in contact with the electrolyte, circuit parameters like voltage, current, capacitance, inductance and frequency of sparking and maximum number of sparks per second.

The numerical value of Q in Cal/s, generated in ECD microwelding, was evaluated with reference to Basak's[2] work on ECDM.

3.2.3(a) HEAT INPUT RATE Q in Cal/s

The heat input rate depends upon the amount of heat released by a single spark. The amount of heat released per spark in Cal/s can be expressed as

$$q = \frac{1}{2} [L(I_c - I_m)^2 + C(V_m - V_c)^2] \lambda_1 \quad (3.7)$$

where L = inductance of the circuit in Henry,

C = capacitance of the circuit in Farad,

I_c = current at the initiation of discharge in ampere,

I_m = instantaneous current at intense discharge condition,

V_m = applied potential at the time of melting in Volts,

V_c = applied potential at the initiation of discharge,
 and λ_1 = spark energy efficiency factor = 1.0 (assuming no
 convective heat transfer)

CONCEPT OF RING SPARK:

Appropriate data for the energy density in the discharge channel are not available in the literature on switching phenomenon. Therefore, relevant data available from the analysis of spark discharge during EDM were used. In EDM the spark channel diameters range from 0.005 cm to 0.03 cm with the energy per spark in the range of 0.1 J to 0.5 J. In ECD microwelding process severe sparking occurs leading to an arcing condition with high energy density. Therefore the larger spark channel diameter was considered to account for the maximum spark energy density; which will strike on the circumference of wire electrode as shown in adjacent figure.

Therefore number of sparks around the circumference of the wire electrode (assuming all sparks occur simultaneously) would be

$$N_{\text{spk}} = \frac{\pi(D + d_{\text{spk}})}{d_{\text{spk}}} = \pi \left[\frac{D}{d_{\text{spk}}} + 1 \right] \quad (3.8)$$

N_{spk} = Maximum number of sparks which can be

simultaneously accommodated around the circumference of the electrode edge.

D = Diameter (equivalent) of twisted wire,

d_{spk} = Diameter of individual spark channel,

Based on above arguments N_{spk} is considered in the range of 3 to 7.

Now the relation to evaluate the frequency of spark generation is taken from Basak's [Refer Appendix-2] work, which is as follows:

$$\gamma_u = \frac{(R_{2c} + 0.5R_{3c})}{L \ln \left\{ 2 \frac{(R_{2c} + R_{3c})}{R_{3c}} \right\}} \quad (3.9)$$

where R_{2c} and R_{3c} are the resistance of electrolyte and the resistance between wire electrode and electrolyte due to vapour blanketing respectively.

Therefore heat input rate is

$$Q = 0.5 [L(I_c - I_m)^2 + C(v_m - v_c)^2] \times N_{spk} \times \gamma_u \quad (3.10)$$

where

L = inductance of the circuit in Henry,

C = capacitance of the circuit in Farad,

I_m = circuit current when melting taken place in Amps,

I_c = circuit current at the initiation of discharge in Amps,

V_m = applied potential when melting occurs in Volts,
and V_c = applied potential when discharge starts in Volts,

3.2.3(b) DETERMINATION OF SPARKING FREQUENCY:

Equation 3.9 shows the expression for sparking frequency. This can be evaluated when the values of R_{2c} , R_{3c} and L are known. In the present case $L = 0.8H$. To find out R_{2c} and R_{3c} , the empirical relations developed by Basak (Appendix-2) is used which are as follows:

For NaCl electrolyte

$$R_{2c} = (0.22MF^{-0.5})/A_e$$

$$R_{3c} = (0.055MF^{-1.0})/A_e$$

where MF = mole fraction of electrolyte

A_e = equivalent area of wire electrode in contact with electrolyte.

This equivalent area is expressed as

$$A_e = \pi.D.l_{eq} \quad (3.9)$$

where l_{eq} = equivalent length of immersion (Refer Appendix-2)

3.2.3(c) DETERMINATION OF CRITICAL CURRENT I_c AND CRITICAL VOLTAGE V_c

The determination of critical current I_c and critical voltage V_c is done with reference to Basak[2]. The procedure is explained in Appendix-2.

$$I_c = (-\gamma + \gamma^2 + 4\sigma R_{3c} A_e \bar{\dot{V}}_c)^{0.5} / 2\sigma R_{3c} \quad (3.10)$$

$$V_c = I_c (R_{2c} + R_{3c}) \quad (3.11)$$

where

γ = electrochemical equivalent of H_2 at $100^\circ C$
expressed in volume = $0.16 \text{ cm}^3/\text{A} - \text{sec}$;

σ = coefficient of vapour formation = 0.018
 $\text{cm}^3/\text{watt-sec}$.

$\bar{\dot{V}}_c$ = (hydrogen gas + vapour) combined gas generation
rate/unit area-sec = 6.28 cm/sec .

3.3 EXPERIMENTAL VERIFICATION OF THE MODEL

The simplified model presented in the previous section of the cylinder face yields the time taken for the centre to reach the melting temperature and the nature of variation of temperature with time.

3.3.1 EXPERIMENTAL SETUP:-

The experimental set-up (shown in Fig2.1) used in the previous experiments was also used for the verification of the ECDW-temperature model. In these experiments the difference in emf recorded by the thermocouple wires was monitored on one channel of the dual channel storage oscilloscope. The other channel recorded the current waveform variation.

Initially several methods were tried to record the nature

of variation of temperature rise. Both the thermocouple wires were twisted and cut orthogonally to produce a flat bottom. This would give a circular peripheral heat source orthogonal to the vertical wire axis. The twisted configuration was dipped upto 2mm into the electrolyte and the twisted length was maintained exactly 4mm with the direction of twisting same to have identical inductance effect. The standard chromel-Alumel thermocouple wire of 0.4mm diameter was used in these tests.

This arrangement showed the emf difference and the nature of temperature-time curve. But the recorded magnitude of the emf showed there would be melting of wire as the calibrated temperature was above the melting temperature of thermocouple wire (Chromel-Alumel).

The extra emf recorded due to non thermoelectric effect might be explained as follows. The negative terminal of the twisted configuration of wire was connected to the main circuit in which heavy current flows. Furthermore the twisting of wire produces some inductive effect. So these two factors were possibly responsible for extra emf recording.

3.3.2 MODIFIED EXPERIMENTAL METHOD: -

Therefore a modified approach was developed. In this case the thermocouple bead was prepared by microwelding using ECD. The bead dimension was maintained of a standard thermocouple;

i.e. the diameter (size) of this bead was made thrice the diameter of the original individual wire. Then the spherical bead of thermocouple was reduced to flat bottom by rubbing off with emery paper. The reason being to achieve a circular flat surface as required in the theoretical model. This thermocouple was now connected in the circuit and dipped just 0.4mm inside the electrolyte. The applied voltage was monitored as it was done in the previous experiments.

The applied voltage and the corresponding current waveform was recorded by the dual channel storage oscilloscope. The current waveform showed the frequency of discharge and its order of magnitude.

When applied voltage varied between 60-70V there was intense sparking almost similar to arcing. The discharge time was seen (from fluctuating current waveform) to be of the order of 10^{-4} sec. In this condition there was no wire melting. At this particular condition the emf difference between the thermocouple wires and the current waveform was recorded by dual channel storage oscilloscope. The recorded emf variation with time and current waveform are shown in Fig.3.3.

The oscilloscope control knobs were kept at autoswitch off and sweepmode position. So it could record the waveforms for a single sweep only as soon as power was switched on.

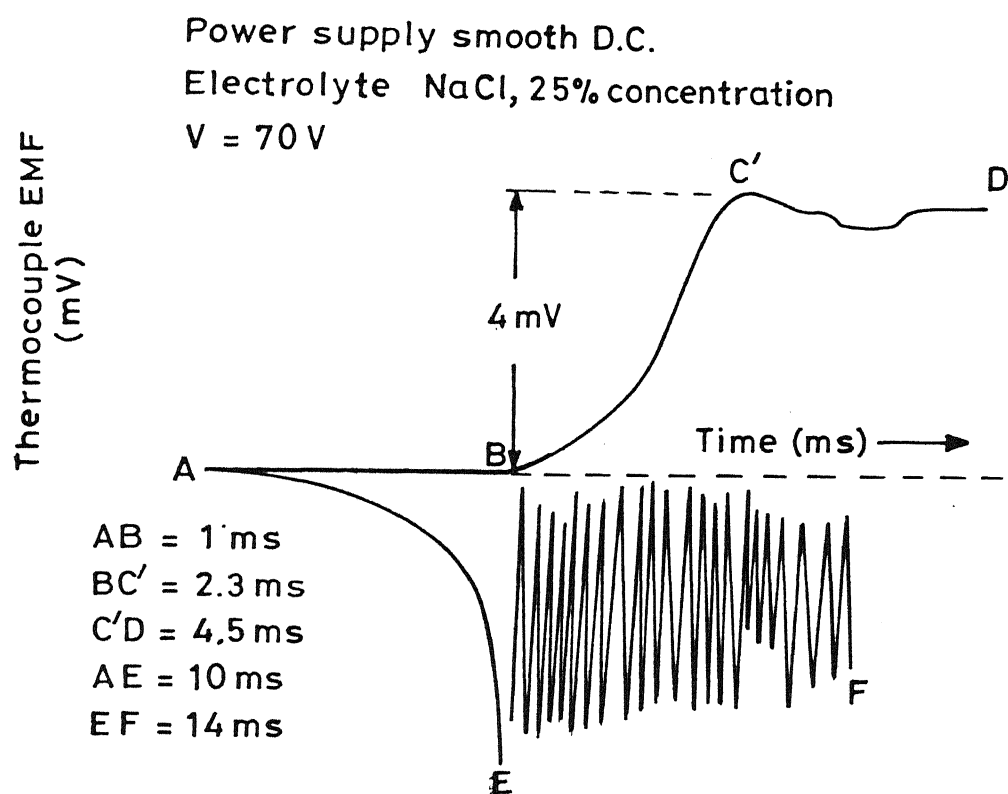


Fig. 3.3 Procedure for measurement of time required by cathode wire to reach the melting temperature

In the oscilloscope there is one frequency control knob. Since the time required for the bead centre to reach melting temperature was in milisecond order the frequency knob was adjusted to milisecond scale. Where as the discharge time was in 10^{-4} sec. order. So the current waveform could not measure discharge time simultaneously. This was checked and confirmed before using the same applied voltage range.

3.3.3 EVALUATION OF THE TIME FOR BEAD CENTRE TO ATTAIN MELTING TEMPERATUR:

So the evaluation of temperature with respect to time was done as shown in Fig. 3.3 Referring to the Fig.3.3, The time recorded from A-B shows the lagging time between the switching of the power and ECD to start. E-F shows the instence sparking condition to ensure the heat input was almost constant. B-C was the actual temperature-time curve when heat input was almost constant (E-F stage). C-D shows the temperature was almost constant with little variation.

The actual temperature-time curve was traced as in Fig.3.4(a) and was super imposed on theoretical curve calculated from the model. The experimental curve then extraplotted to find out the exat time required to reach the melting temperature as shown in Fig.3.4(b). Because the thermocouple at molten stage generates very little emf.

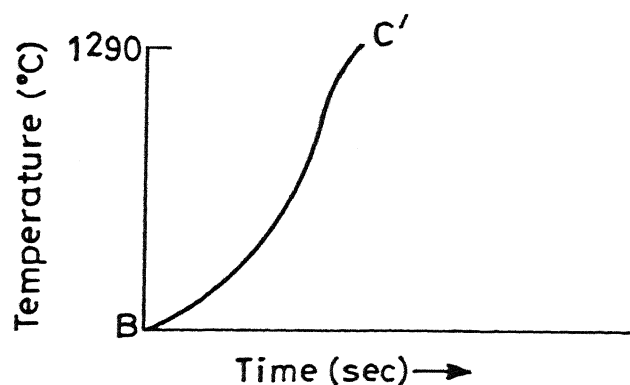


Fig. 3.4(a) Variation of temperature w.r.t. time obtained experimentally

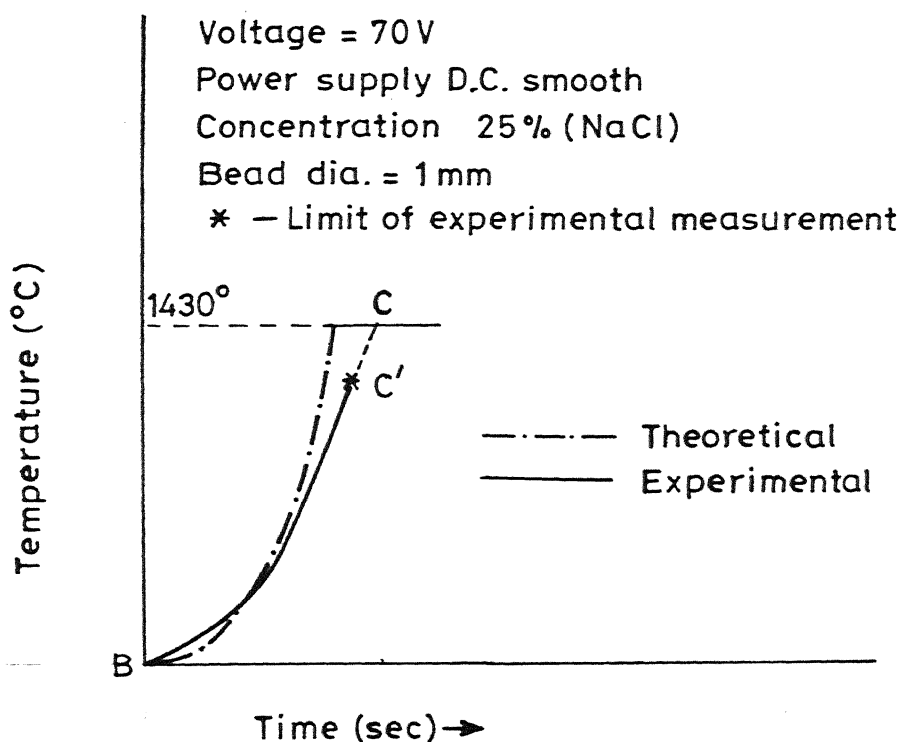


Fig. 3.4(b) Comparison of observed and calculated time for cathode wire to reach melting point.

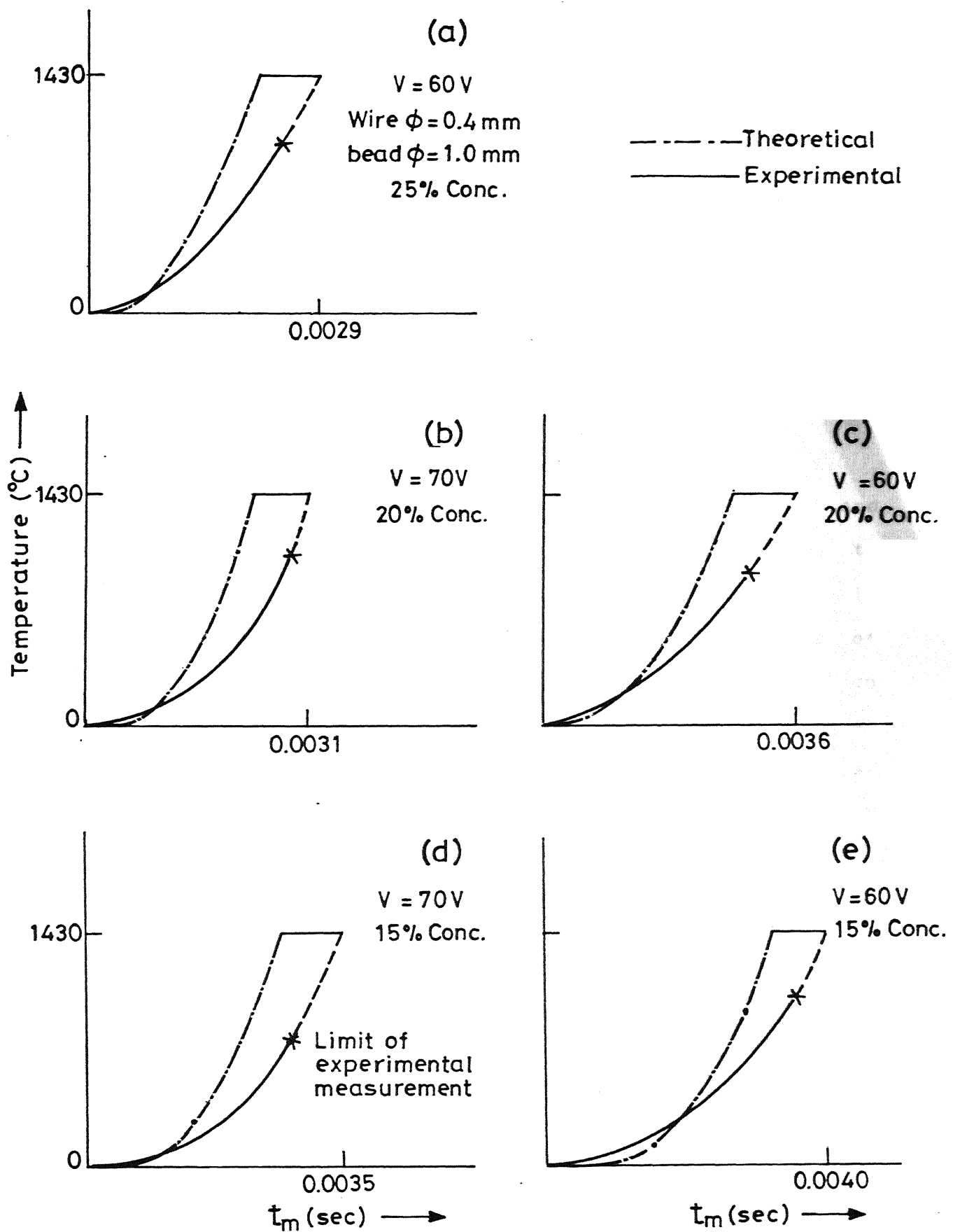


Fig. 3.5 Experimental and theoretical pattern showing nature of variation of temperature with time in ECD microwelding.

The temperature-time curve were recorder for three concentration of NaCl i.e. 15%, 20% and 25%. It was also recorded for two applied potential values of 60V and 70V for which there was intense sparking, but no melting. (Refer Fig.3.5a-e).

3.3.4 EFFECT OF DIAMETER ON MELTING TIME

Various diameters of chromel-Alumel wires were tried and the time taken to reach the melting temperature with respect to diameter size was estimated and plotted as shown in Fig.3.6. In figure (3.7a-3.7b) both experimental and theoretical values of t_m (time taken by the bead centre of thermocouple wire to reach the melting temperature) were plotted and compaired against different concentration of electrolyte at two different applied voltages.

3.3.5 EFFECT OF APPLIED VOLTAGE AN CONCENTRATION:

Figure 3.8 shows the nature of variation of t_m vs applied voltage at different electrolyte concentration . Calculated theoretically where as (Fig.3.9) shows the experimental results and it was compared in following Fig. 3.9

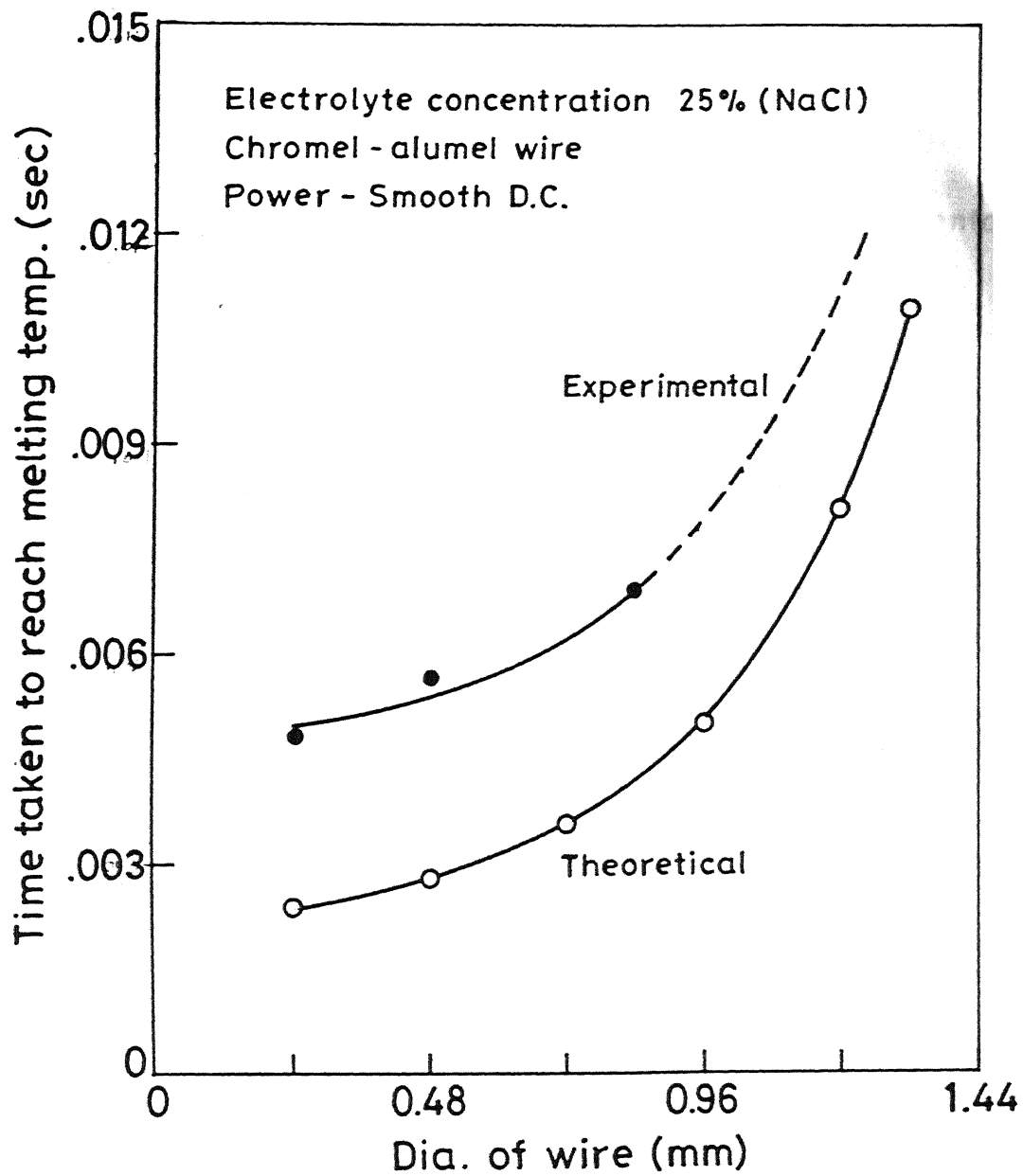


Fig. 3.6 Time to reach melting temperature of wire as a function of wire diameter.

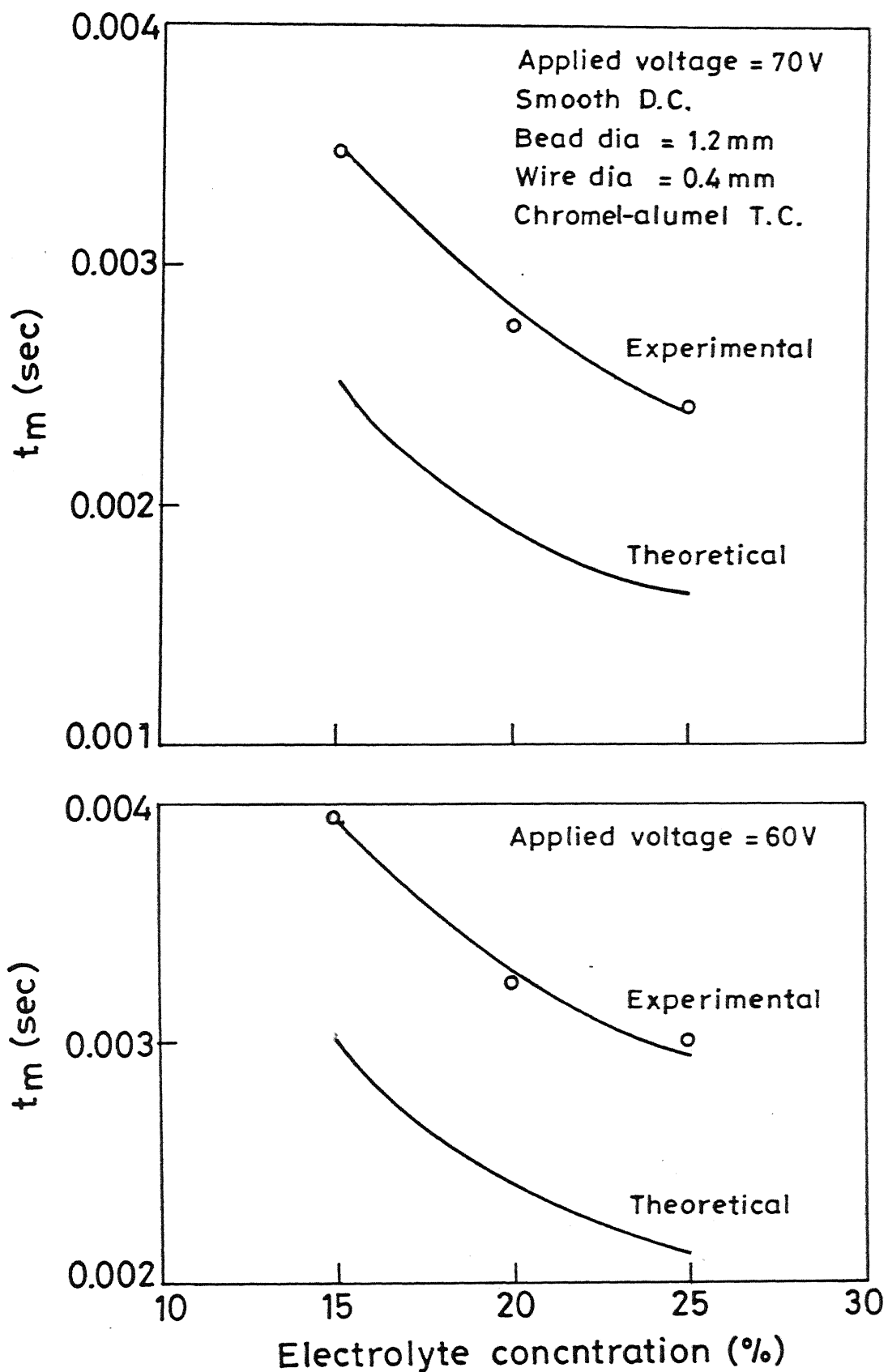


Fig. 3.7 Time to reach melting temperature vs electrolyte concentration (NaCl)

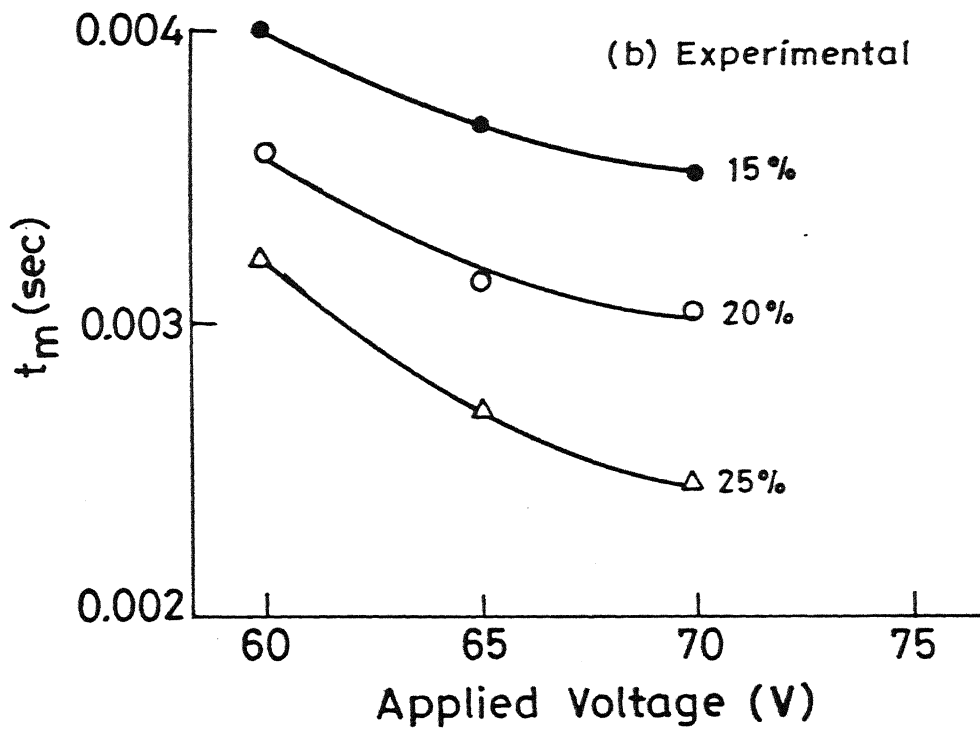
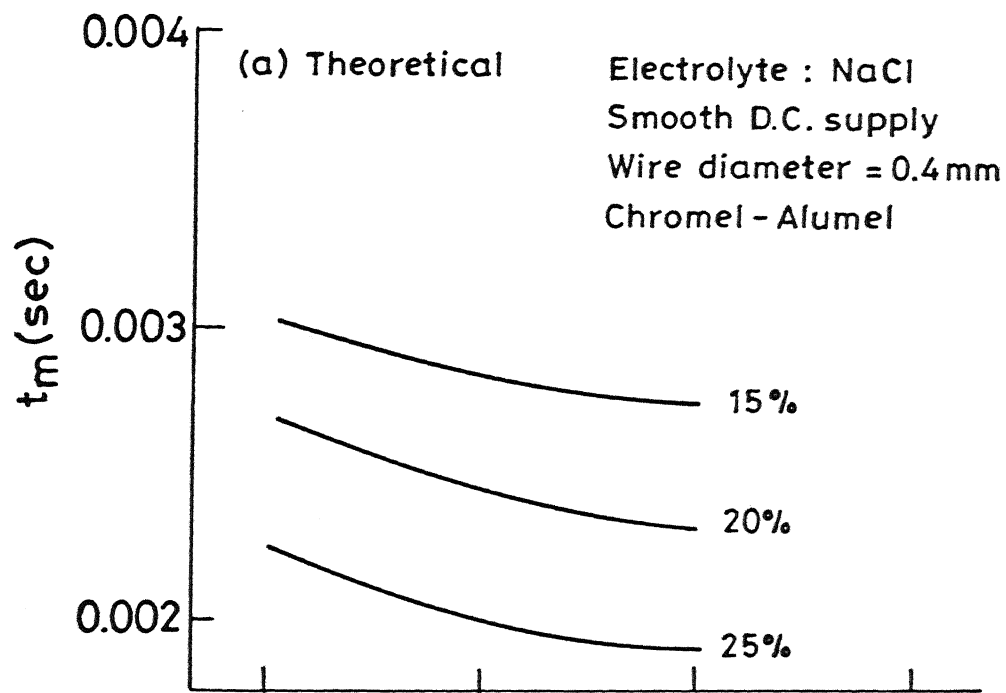


Fig. 3.8 Variation of t_m with applied voltage at different concentration.

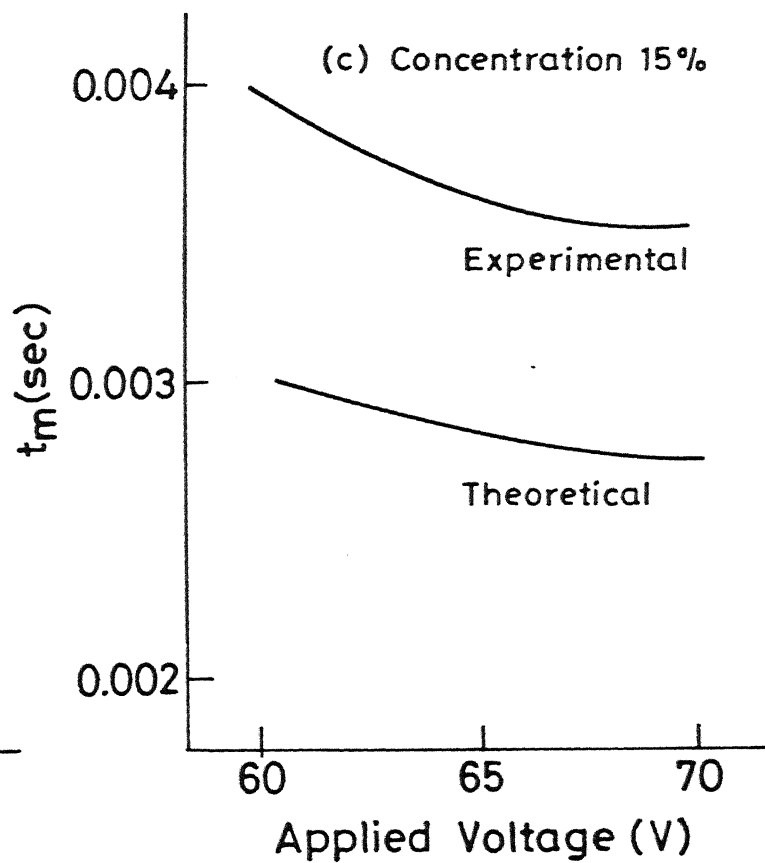
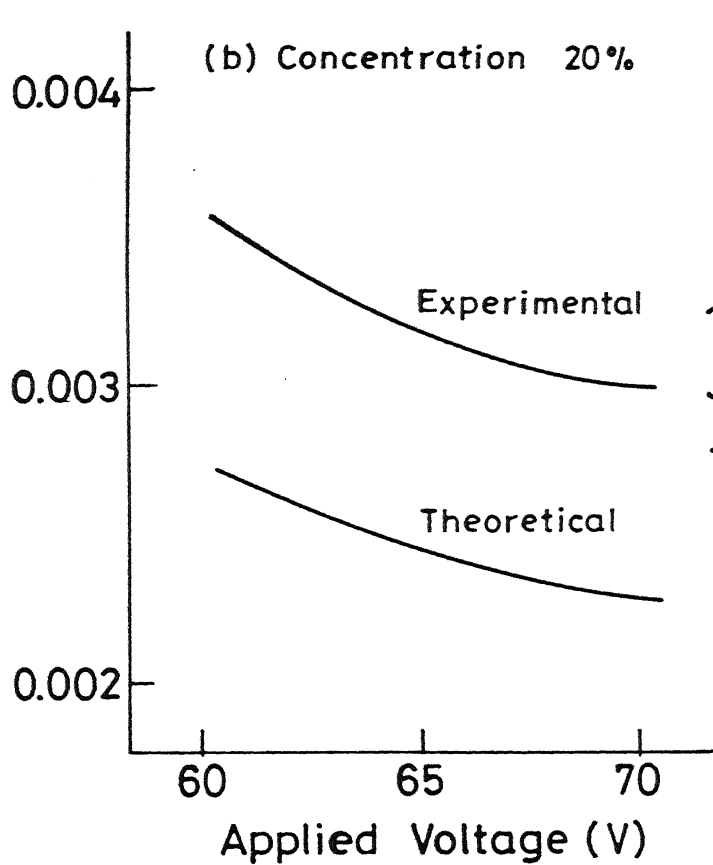
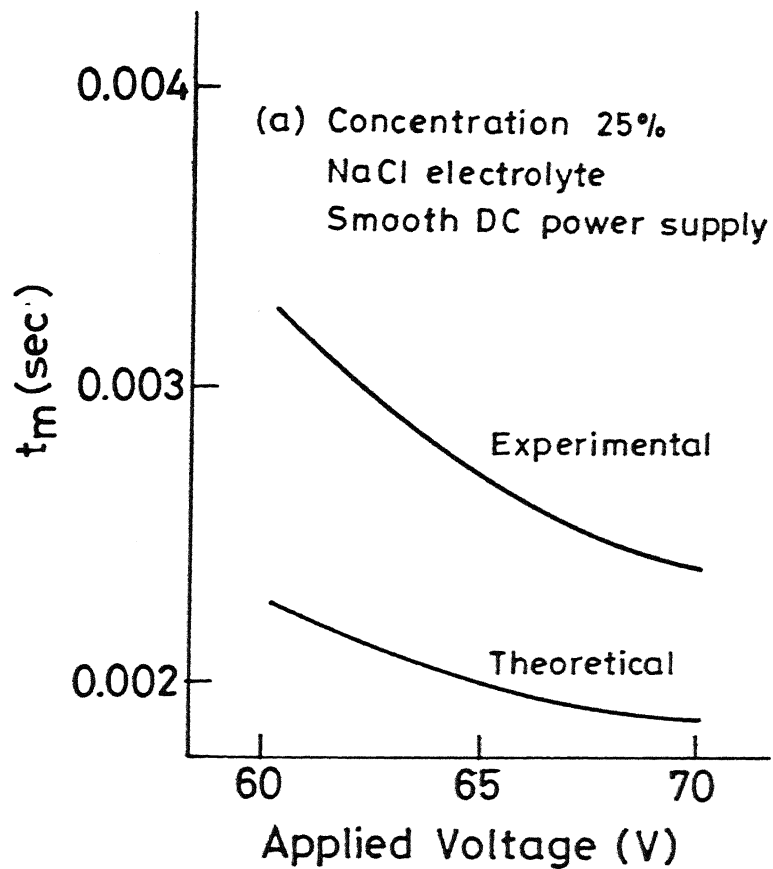


Fig. 3.9 Comparison of t_m vs applied voltage at different electrolyte concentrations.

3.4 SUMMARIZATION OF THE RESULTS:

The accuracy of the model developed was examined by comparing the characteristics obtained on the basis of the model with those obtained from the experiments. The model indicates that the melting temperature attained by the cathode wire is a function of thermal conductivity, thermal diffusivity, density, specific heat etc. It also depends upon type and concentration of the electrolyte, the wire diameter, depth of immersion of wire in electrolyte; the circuit parameters like capacitance, inductance and applied voltage. So from the results it was found that the important assumptions made in developing the model were reasonably acceptable. Little error in the experimental curves were due to extrapolation to determine the actual time required for the bead centre to attain melting temperature.

CHAPTER IV

CONCLUDING REMARK AND SCOPE FOR FUTURE WORK

This chapter contains the discussion on the process characteristics of microwelding using ECD. Few comments on the thermal aspect of microwelding are also included in this chapter. Finally, the limitations found in the present work and the suggested course of future work are also presented.

4.1 DISCUSSION ON THE RESULTS OBTAINED FROM ECD MICROWELDING EXPERIMENTS

(i) The results obtained from an elaborate set of experiments show that the intensity of discharge is very high when the power supply is smooth D.C. with both inductance and capacitance present in the circuit. The discharge frequency is also very high, which could be seen from the current waveform (Fig. 2.5d). The capacitor in the circuit increases the energy release per spark. The melting of the wire takes place when the voltage is above 80 volts. So, at this applied voltage the sparking is almost continuous and the released of heat could be considered to be uniform.

(ii) Figure 2.7 shows the depth of immersion vs wire diameter for different materials. The exponential nature of

variation of the graph can be explained as follows. As the wire diameter increased the cross sectional area increased proportional to square of the diameter. Both the wires are also twisted which increased the volume of the wire material for given depth of immersion.

(iii) It could be also observed that for a particular wire diameter the optimal depth of immersion varies for different wire materials. This happens because the buoyant force due to electrolyte also plays a major role in bead formation. For a particular bead diameter ($\sim 3d$) the copper wire combination is dipped to lesser depth compared to Chromel-Alumel combination.

(iv) Surface tension force, ' F_T ', buoyant force ' F_B ', force due to gravity, F_g , and the intensity of discharge on molten metal pool are the governing factors, which affect the optimum size besides the process parameters discussed earlier. In case of platinum wires surface tension is very high compared to F_B and F_g . So the depth of immersion is low.

(v) From Fig. 2.7(a) it could be concluded that microwelding is possible with higher wire diameters only for identical materials, but for different material composition only

thinner wires can be welded. The reason being metallurgical phase change and heterogeneous distribution of metals at molten state and quick solidification of bead due to volumetric contraction.

(vi) Figure 2.13 depicts the satisfactory combination range of concentration and applied voltage for ECD microwelding. This is found for the diameter range of 0.12 to 1.2 mm of Chromel-Alumel wires. This shows that at a particular applied voltage different wire diameters can be welded even if the electrolyte concentration varies as the process continues. This is very useful for industrial application. It is also clear from the figure that the performance with a smooth D.C. is better.

4.2 DISCUSSION ON THERMAL MODEL: THEORETICAL AND EXPERIMENTAL ASPECTS

The thermal model, developed to find out the time taken to reach the melting temperature, was discussed in the previous chapter. Comparison of theoretical and experimental time to reach the melting temperature as shown in Fig. 3.4 (b) and Fig. 3.5(a)-(e) show a reasonably good agreement. When the concentration is high (25%) the variation in the theoretical and observed melting time is less compared to that with lower concentration (15%). This is because as the concentration

increases conductivity of electrolyte also increases so that resistivity values (R_{2c} and R_{3c}) decrease. Thus, at higher concentration the spark energy intensity also increases resulting in lesser time to reach the melting temperature. The experimentally observed temperature rise curves deviate a little bit from the theoretically estimated trends. This could be due to the idealised conditions considered in theoretical model as constant resistivity between the electrolyte and wire, constant frequency of discharge and concept of ring spark as the ring heat source. Thus it is apparent that at a time a major part of the edge is sparking.

Figure 3.6 shows that the theoretical melting time is less compared to the experimental time and it increases as the diameter of the wire increases. The difference between the theoretical and experimental values of the time reduce at higher diameters. It could be due to a somewhat slow response by thicker wires.

Figure 3.7 shows that at a particular applied potential the melting time, t_m decreases with concentration because the rate of heat release increases with concentration. Figure 3.8 again confirms that as the applied potential increased the spark intensity and the frequency of sparking also increased resulting in the less t_m .

4.3 LIMITATIONS OF THE PRESENT WORK AND SCOPE FOR FURTHER RESEARCH

The main objective of the present work was

- (a) to identify the influences of optimum process parameters to obtain a satisfactory welded bead by ECD microwelding and
- (b) to find out the time required for completion of welding (which is indicated by the time required by the wire to reach the melting temperature. A number of assumptions were made in thermal analysis of the process. Though the results were in close agreement showing the model to be reasonably acceptable further work could not be taken up due to lack of time and facilities available. Considering these future research can be extended in the following direction.

- (i) The exact nature of severe sparking when the wires reach melting condition and the frequency of (sparking) discharges should be determined precisely. This can be done by using high speed cinematographic technique.
- (ii) Estimation of total time taken for the welding process to complete; i.e. to develop a thermal model considering a moving heat source and then experimental

verification of the model can be developed and verified.

(iii) Formulation of a theoretical model of the molten bead predicting the interrelation between the metallurgical phenomenon (such as volumetric contraction from fluid to solid, volumetric dilatation, material composition and the latent heats associated with melting and solidification of the bead) and the residual stress.

(iv) The effect of surface tension, gravity force and buoyancy force on bead formation should be investigated in detail leading to a theoretical estimation of the optimal depth of immersion.

REFERENCES

1. Allesu K. - Ph.D. Dissertation, IIT - Kanpur (India), 1988.
2. Basak I. - Ph.D. Dissertation, IIT - Kanpur (India), 1992.
3. Allesu K., Umesh N.K., Muju M.K., Ghosh A. - 12th AIMTDR conference, IIT Delhi, 1986.
4. Umeshkumar N - M.Tech. Thesis, IIT- Kanpur (India), 1985.
5. Janseen L.J.J., Hoogland J.G. - Electrochim Acta, V15, P.1013, 1970.
6. Cook N.H., Foote G.B., Jordan P., Kalyani B.N. et.al Journal for Industry, P945, 1973.
7. Kellog H.H. - Jl. of Electrochemical Soc. n. 97, p.133, 1950.
8. Ghosh A., Basu B. - Jl. of Technology, VXI. n.1, 1966.
9. Allesu K., Ghosh A., Muju M.K. - European Jl. of Mech. Engg., V36, n.3, 1991.
10. Sheng C.I., Cheny Y. - Jl. of Engineering material and Technology - V114 - pp.439 - Oct, 1992.
11. El - Hofy H., McGeough J.A. - Trans ASME, Jl. of Engg. for Inds., n.110, p.119, 1988.
12. McGeough J.A., Khayry A.B.M., Munro W. - Annals of CIRP, V32, n.1, p.113, 1983.
13. Khayry A.B.M., McGeough J.A. - proc of 25th IMTDR, London,

p321, 1985.

14. McGeough J.A., Desilva A. - Proc Inst. of Mech. Engg., V200, nB4, p237 1986.
15. NI X. W. McGeough J.A. - Winter Annual Meeting of ASME (PED - V34), p63, 1988.
16. Drake T.H., McGeough J.A. - Proc. 22nd IMTDR. UMIST p361. 1981.
17. Tsuchiya, Inoue, Miyazaki. et.al - Bull. Jap. Soc. of Prec. Engg. V 19, n 1 p73 1985.
18. Prentice G. - "Electrochemical Engineering Principles" - PHI, (1991).
19. Basak I., Ghosh A. - Mechanism of Spark Generation in during ECDM: A theoretical model and experimental verification - (communicated for publication).
20. Carslaw H.S., Jaeger J.C. - "Conduction of Heat in Solids". Oxford at the Charendon Press (2nd Edn., 1959).
21. Myers G.E. - "Analytical Methods in Conduction Heat Transfer" McGraw Hill, p.491, (1971).
22. Perry R.H., Chilton C.H. - "Chemical Engineering Handboob", McGraw Hill, (5th Edition).
23. Holm R. - "Electrical Contacts, Theory and Application" 4th Edition, (1981).
24. IIDA T., Guthrie R.I.L - "The Physical Properties of Liquid Metals", Oxford Sc. Publication, (1988).

25. OMEGA Standard Temperature measurement and calibration Handbook.
26. ASM Metals Handbook V-16, 1984.
27. ASM Metals Handbook V-17, 1984.

APPENDIX-I

PROBLEM FORMULATION (Referring 'CONDUCTION OF HEAT IN SOLIDS' - by CARSLAW AND JAEGAR)

The problem is formulated for rectangular co-ordinate system

The temperature $T(x, y, z, t)$ due to a instantaneous point source at (x', y', z', t) in an infinite medium is

$$T_{(x, y, z, t)} = \frac{1}{8(\pi\alpha t)^{1.5}} e^{-[R^2 + (z-z')^2]/4\alpha t} \quad (A.1)$$

$$\text{Where } R^2 = (x-x')^2 + (y-y')^2$$

$$= r'^2 + r^2 - 2rr' \cos(\theta - \theta')$$

and (r, θ) , (r', θ') are the polar co-ordinates of the points (x, y) , (x', y') .

Using the laplace transform technique where we have

$$\begin{aligned} \bar{T} &= \frac{e^{-q\sqrt{[R^2 + (z-z')^2]}}}{4\pi\alpha [R^2 + (z-z')^2]} \quad (A.2) \\ &= \frac{1}{2\pi^2\alpha} \int_0^\infty \cos \xi(z-z') k_0(\eta R) d\xi \end{aligned}$$

$$\text{Where } \eta = \sqrt{\xi^2 + q^2} \quad A.3$$

CYLINDRICAL CO-ORDINATE SYSTEM

We consider first the temperature at the point (r, θ, z) in cylindrical co-ordinates due to a unit instantaneous point source at $t = 0$ at the point $(r', \theta', 0)$ the surface $r = a$ being kept at zero temperature.

In this case we start with the form A-2 and use the Addition theorem for Bessel function $K_0(\eta R)$ which occur in is

$K_0(\eta R)$ is defined

$$K_0(\eta R) = \sum_{n=-\infty}^{\infty} \cos n(\theta - \theta') I_n(\eta r) K_n(\eta r') \quad r < r'$$

$$K_0(\eta R) = \sum_{n=-\infty}^{\infty} \cos n(\theta - \theta') I_n(\eta r) K_n(\eta r') \quad r > r' \quad A.4$$

Usually we seek a solution $T(r, \theta, z, t) = u + w$, where w satisfies the differential equation of conduction of heat and to vanish for $t = 0$, and to be such that u satisfies the boundary conditions. The subsidiary equation for 'w' is

$$\frac{1}{r^2} \frac{\partial^2 \bar{w}}{\partial \theta^2} + \frac{\partial^2 \bar{w}}{\partial r^2} + \frac{1}{r} \frac{\partial \bar{w}}{\partial r} + \frac{\partial^2 \bar{w}}{\partial z^2} - q^2 \bar{w} = 0 \quad (A.5)$$

and to be bounded at $r = 0$ and such that

$$\bar{u} + \bar{w} = T(r, \theta, z, t) = 0 \quad \text{where } r = a; \text{ thus}$$

$$\bar{w} = - \frac{1}{2\pi^2 \alpha} \sum_{n=-\infty}^{\infty} \cos n(\theta - \theta') \int_0^{\infty} \cos \xi z \frac{I_n(\eta r) I_n(\eta r') K_n(\eta a)}{I_n(\eta a)} d\xi.$$

It follows that if $r < r'$

$$T(r, \theta, z, t) = \frac{e^{-z^2/4\alpha t}}{2\pi a^2 \sqrt{\pi \alpha t}} \sum_{n=-\infty}^{\infty} \cos n(\theta - \theta') \sum_{\lambda} e^{-\alpha \lambda^2 t} n \sum \frac{\lambda J_n(\lambda r) J(\lambda r')}{\lambda [J'_n(\lambda a)]^2} \quad (A.8)$$

when $z = 0$ the temperature at $T(r, \theta, z, t)$ when the radiation into a medium is then

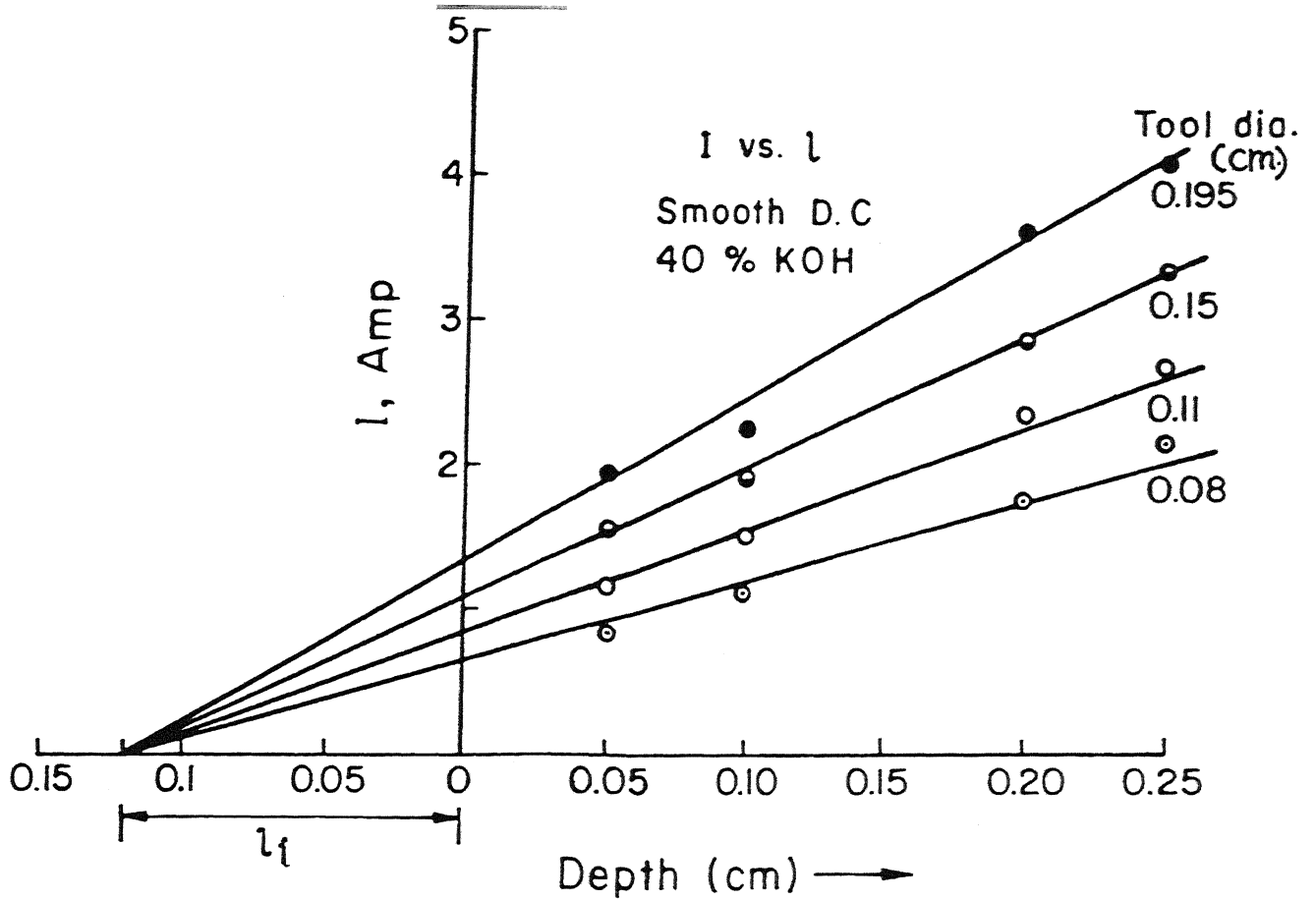
$$T(r, \theta, z, t) = \frac{e^{-z^2/4\alpha t}}{2\pi a^2 \sqrt{\pi \alpha t}} \sum_{n=-\infty}^{\infty} \cos n(\theta - \theta') \sum_{\lambda} e^{-\alpha \lambda^2 t} n \sum \frac{\lambda J_n(\lambda r) J(\lambda r')}{\lambda [J_n^2(\lambda a)](\lambda^2 + h^2 - x^2/a^2)} + \frac{e^{-z^2/4kt}}{2a^2 \pi (\pi \alpha t)^{1/2}} \quad (A.9)$$

APPENDIX - 2

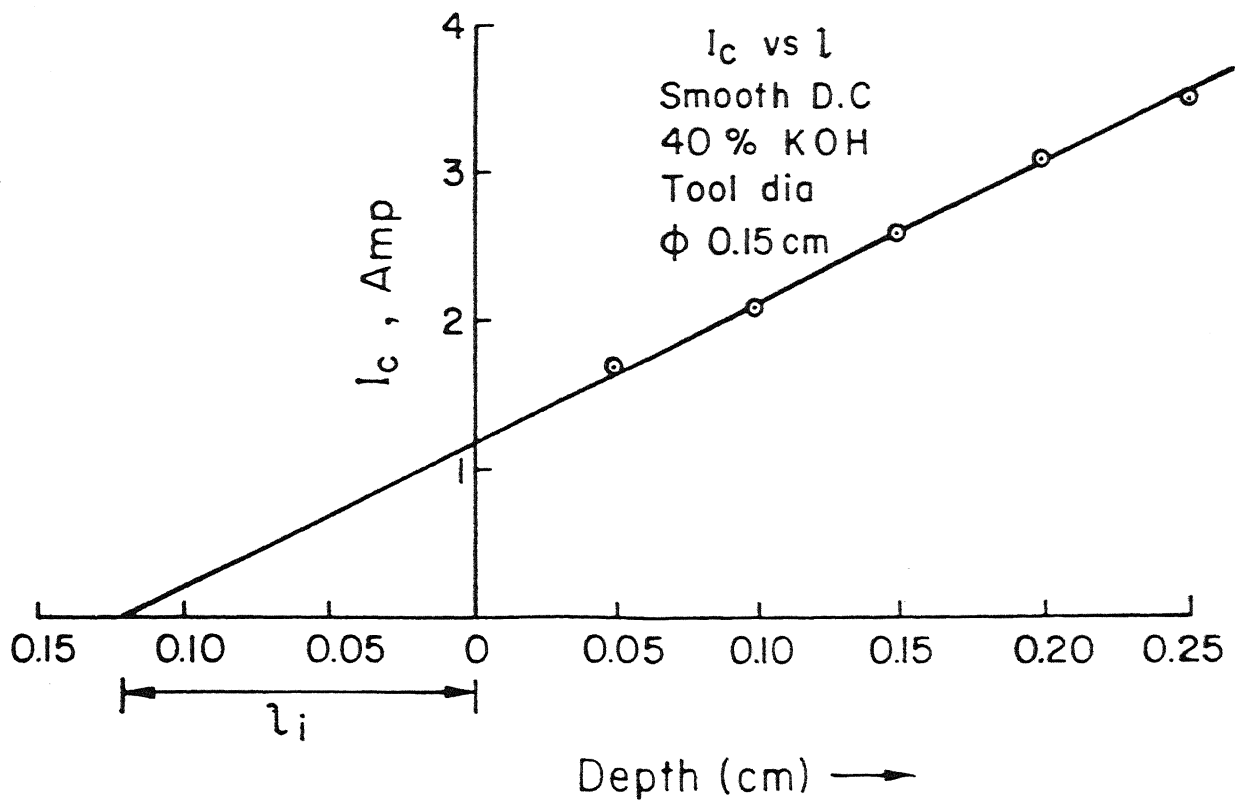
The experimental setup described earlier was used for conducting the pilot experiments for determining the values of the required constants and critical parameters such as l_i and the critical resistances at different regions of the electrochemical cell.

Evaluation of l_i

To determine l_i , different diameters of electrodes were used and 15V smooth DC supply was applied to the cell; the resulting current through the circuit was noted for different depths from 0.05 cm. to 0.25 cm. The obtained straight lines intercepted the X - axis (depth axis) at $x = - 0.12$ cm. in all cases. This intercept represents l_i (Fig. A1). This magnitude remains same for all electrolytes and also at the critical condition (Fig. A1). It indicates that at the edge of electrode the current distribution remains unchanged relative to other part of the active electrode surface, for any depth and an additional imaginary length, equal to the intercept, can be assumed, on which the effective current density is identical with the rest of the length.



(a)



(b)

Fig.A.1 Evaluation of l_i

Evaluation of critical reactances:

Out of the three components of the total resistance at the critical stage it was found that R_{1c} is much smaller compared to R_{2c} and R_{3c} owing to the low bubble density at the larger electrode surface and can be neglected. The resistance of the bulk electrolyte (R_2) depends primarily on the electrolyte concentration and the geometric configuration of the wire electrode. It was noted that the interelectrode distance has very low effect on this, probably due to the strong concentrations of electrolytes used and high applied potential. Therefore, R_2 is independent of voltage applied and constant throughout and can be taken as R_{2c} . On the otherhand R_{3c} depends on the geometrical configuration of wire electrode, electrolyte concentration and the bubble density on the surface of the wire electrode. Since, the bubble density at the electrode surface is a function of the applied potential, to determine R_{3c} , the concerned experiments were required to be done at the critical condition. The dependence of R_{2c} and R_{3c} on the electrolyte concentration and the active equivalent surface area, were found to follow the relations given below:

$$R_{2c} = K_2 M^{\lambda_2} / A_e, \text{ and}$$

$$R_{3c} = K_3 M^{\lambda_3} / A_e.$$

where, M is the mole fraction given by,

$$M = \frac{m_2}{m_1 + m_2}$$

with m_2 as the moles of the solute present in m_1 moles of the solvent (water). K_2 , K_3 , λ_2 and λ_3 are constants and to be determined by the pilot experiments.

To determine R_2 ($= R_{2c}$), i.e., K_2 and λ_2 , a rectified low D.C. voltage was applied and the corresponding current was recorded by a dual channel storage oscilloscope. Since, the bubble generation rate is low at the electrodes under such the condition, R_3 can be neglected, and R_2 can be found out as the ratio of the instantaneous voltage and the instantaneous current. This ratio was determined at a few points of the voltage - current traces and it was found that the ratio ($=R_2$) remains practically constant. This procedure was repeated for gradually increased voltage steps and it was found that beyond a certain value of the peak voltage applied, the current trace distorts, implying increased bubble generation rate at the electrode leading to the development of a significant resistance at the smaller electrode-electrolyte interface (R_3). The mean value of the ratio of the voltage-current traces at different points, (with undistorted current traces) was taken as the value of R_2 . Repeating this with different concentrations K_2 and λ_2 values were determined.

For each concentration level of electrolyte the total resistance at the critical condition, $R_c (=R_{2c}+R_{3c})$ was determined as the ratio of the critical voltage and the critical current. Thus R_{3c} can be expressed as

$$R_{3c} = R_c - R_{2c}$$

Again the values of K_3 and λ_3 were determined from experiments with different electrolytes.

The value of the constants are tabulated below.

Electrolyte	K_2 $\Omega \text{ cm}^2 \text{ mole}^{-0.5}$	K_3 $\Omega \text{ cm}^2 \text{ mole}^{-1}$	λ_2	λ_3
NaCl	0.22	0.055	-0.5	-1.0

Evaluation of \bar{v}_c and δ :

The other two invariants to be evaluated were \bar{v}_c and δ . A different set of pilot experiments were conducted with different configurations and corresponding values of R_{3c} , A_e , α and J_c were substituted in the following expression. Solving the resulting quadratic equations \bar{v}_c and δ were found to be 16.05 cm/sec. and 0.048 cm³/watt-sec. respectively.

$$\delta \cdot R_{3c} \cdot A_e J_c^2 + \alpha \cdot J_c - \bar{v} = 0$$

where, α = Coefficient of Faradic H_2 gas generation = 0.23
 $cm^3/A\text{-sec.}$, δ = Coefficient of thermal vapour generation = 0.048
 $cm^3/watt\text{-sec.}$, $\bar{v}_c = H_2 + \text{water vapour generation rate per unit}$
area = 16.05 $cm/sec.$